



HAL
open science

A filtered multilevel Monte Carlo method for estimating the expectation of discretized random fields

Jérémy Briant, Paul Mycek, Mayeul Destouches, Olivier Goux, Serge Gratton, Selime Gürol, Ehouarn Simon, Anthony Weaver

► To cite this version:

Jérémy Briant, Paul Mycek, Mayeul Destouches, Olivier Goux, Serge Gratton, et al.. A filtered multilevel Monte Carlo method for estimating the expectation of discretized random fields. 2023. hal-04337114

HAL Id: hal-04337114

<https://hal.science/hal-04337114v1>

Preprint submitted on 15 Oct 2024

HAL is a multi-disciplinary open access archive for the deposit and dissemination of scientific research documents, whether they are published or not. The documents may come from teaching and research institutions in France or abroad, or from public or private research centers.

L'archive ouverte pluridisciplinaire **HAL**, est destinée au dépôt et à la diffusion de documents scientifiques de niveau recherche, publiés ou non, émanant des établissements d'enseignement et de recherche français ou étrangers, des laboratoires publics ou privés.



Distributed under a Creative Commons Attribution 4.0 International License

A filtered multilevel Monte Carlo method for estimating the expectation of discretized random fields*

Jérémy Briant^{1,2}, Paul Mycek², Mayeul Destouches³, Olivier Goux², Serge Gratton^{1,4},
Selime Gürol², Ehouarn Simon¹, and Anthony T. Weaver²

¹IRIT, UMR 5505 CNRS-INP, Toulouse, France (jeremy.briant@toulouse-inp.fr,
serge.gratton@toulouse-inp.fr, ehouarn.simon@toulouse-inp.fr).

²CECI, UMR 5318 CNRS-CERFACS, Toulouse, France (mycek@cerfacs.fr,
goux@cerfacs.fr, gurol@cerfacs.fr, weaver@cerfacs.fr).


³Met Office, Exeter, UK (mayeul.destouches@metoffice.gov.uk).

⁴ANITI, Toulouse, France.

Abstract

In this paper, we investigate the use of multilevel Monte Carlo (MLMC) methods for estimating the expectation of discretized random fields. Specifically, we consider a setting in which the input and output vectors of the numerical simulators (models) have inconsistent dimensions across the multilevel hierarchy. This requires the introduction of grid transfer operators borrowed from multigrid methods. Starting from a simple one-dimensional illustration, we demonstrate numerically that the resulting MLMC estimator deteriorates the estimation of high-frequency (small-scale) components of the discretized expectation field compared to a (single-level) Monte Carlo (MC) estimator. By adapting mathematical tools initially developed for multigrid methods, we perform a theoretical spectral analysis of the MLMC estimator of the expectation of discretized random fields, in the specific case of linear, symmetric and circulant simulators. This analysis provides a spectral decomposition of the variance into contributions associated with each scale component of the discretized field. We then propose improved MLMC estimators using a filtering mechanism similar to the smoothing process of multigrid methods. The filtering operators improve the estimation of both the small- and large-scale components of the variance, resulting in a reduction of the total variance of the estimator. These improvements are quantified for the specific class of simulators considered in our spectral analysis. The resulting filtered MLMC (F-MLMC) estimator is applied to the problem of estimating the discretized variance field of a diffusion-based covariance operator, which amounts to estimating the expectation of a discretized random field. The numerical experiments support the conclusions of the theoretical analysis even with non-linear simulators, and demonstrate the improvements brought by the proposed F-MLMC estimator compared to both a crude MC and an unfiltered MLMC estimator.

Keywords: Multilevel Monte Carlo, multigrid method, random field, spectral analysis, filtering, diffusion operator.

*  Distributed under a [CC-BY 4.0 licence](https://creativecommons.org/licenses/by/4.0/). This project has received financial support from the CNRS (Centre National de la Recherche Scientifique) through the 80|Prime program and the French national program LEFE (Les Enveloppes Fluides et l'Environnement).

1 Introduction

Monte Carlo (MC) estimation refers to a class of statistical methods that rely on the sampling of random quantities to construct so-called MC estimators. Such estimators are popular and widely-used owing to their simplicity and flexibility. However, their slow convergence in terms of their root mean square error (RMSE) with respect to the sample size makes them inefficient or even unaffordable for the estimation of statistics of outputs of computationally expensive numerical simulators. Alternative techniques often rely on the use of surrogate models, which typically consist of an approximate functional representation of the mapping between the inputs and the output of interest of a numerical simulator. Commonly used surrogate models include, among others, polynomial chaos expansions [34, 37, 42, 62], Gaussian processes [46, 47] or neural networks [54]. Once constructed, such surrogate models are inexpensive to evaluate, so that accurate MC estimators of their output can be obtained at limited computational cost. However, the resulting estimators suffer from model error (bias) coming from the approximation error of the surrogate model with respect to the actual simulator, which may be significant for complex, highly non-linear simulators. In addition, surrogate models generally suffer from the so-called curse of dimensionality, which makes their construction cost grow exponentially with the stochastic input dimension. This curse can, in principle, be mitigated by resorting to model order reduction techniques to lower the dimensionality of the input [45, 51], but this comes at the expense of increasing model error even further.

Another avenue consists of modifying the original, inefficient MC methods to reduce their RMSE. A first class of techniques relies on improving the space-covering of the stochastic input space. Such techniques include Latin hypercube sampling [40] and quasi Monte Carlo methods [35, Chapter 5]. A second class is that of so-called variance reduction techniques [35, Chapter 4], which consist of rewriting the original MC estimator into a transformed estimator with smaller variance (and hence RMSE, provided the bias remains unchanged) for an equivalent computational cost. In recent years, many multilevel/multifidelity estimation methods relying on variance reduction techniques have been proposed in the literature [18, 20, 43, 50]. Among them, the multilevel Monte Carlo (MLMC) method [18, 19, 29] relies on a collection of simulators of different fidelities. In MLMC methods, such fidelities typically correspond to different discrete resolutions, so that the collection of fidelities can be structured as a hierarchy of so-called levels, consisting of simulators of increasing discrete resolution, and hence of increasing accuracy and computational cost. MLMC estimators are constructed by combining samples (or ensembles) from different levels in a particular manner that, under certain assumptions, reduces the variance of the resulting multilevel estimator, while leaving the bias unchanged. The closely-related multilevel best linear unbiased estimators (MLBLUEs) were recently proposed to combine more general multifidelity samples to provide an optimal reduction of the variance [49, 50]. Originally designed for the estimation of the expected value of scalar, real-valued random variables, the MLMC methodology has since been extended to the estimation of higher-order statistical moments [2, 3] and variance-based global sensitivity measures [41]. The analysis of MLMC estimators has also been extended to the estimation of statistics of random variables with values in separable Hilbert spaces [2, 3]. Likewise, strategies for extending MLBLUEs to the estimation of statistical moments of multiple simulator outputs were proposed in [10, 13, 14].

The estimation of a covariance matrix is a prominent example where MLMC approaches have started to emerge, especially in the field of ensemble data assimilation [13, 24, 30]. Another example, which will constitute the motivating example of this paper, is embedded in the general approach of using a discretized linear differential operator to represent the application of a parametric form of a covariance matrix. In particular, we focus on an approach that uses a discretized diffusion operator to represent a covariance operator with a parametric kernel from the Matérn family [53]. Diffusion operators are commonly used for modelling spatial covariances in ocean data assimilation

[58] and are closely related to other techniques for modelling spatial covariances in atmospheric data assimilation [44], geostatistical modelling [36], inverse problems [8] and uncertainty quantification [15]. Central to the approach is the need to extract the diagonal elements (*intrinsic* variances) of the diffusion-modelled covariance matrix so that they can be used to normalize the matrix, to transform it into a (unit-diagonal) correlation matrix. Once the covariance matrix is properly normalized, a desired variance field, different from the intrinsic variance field, can be imposed. The standard method for estimating the intrinsic variances of the diffusion-based covariance matrix is the randomization method [58, 59]. This method relies on the MC estimation of the expectation of a discretized random field, which, in a more abstract formulation, may be viewed as the output of a numerical simulator, whose input is also a discretized random field.

In this paper, we are interested in applying the MLMC methodology to improve the efficiency of estimating the expectation of discretized random fields in the abstract setting described above. To achieve this, certain adaptations of the original MLMC formulation must be made. First, the input and output of the abstract numerical simulator considered in our study are discretized fields, typically represented as n -dimensional vectors for practical, numerical reasons. While multilevel approaches have been proposed in the literature to tackle the case of numerical simulators with vector inputs and outputs [10, 14], such vectors are simply used as a means to collect scalar quantities. However, the components of discretized fields should *not* be considered as individual, separate scalar quantities, precisely because they encapsulate physical and spatial information on the underlying continuous fields that are discretized. We stress that the vectors at hand represent discretized fields and should be thought of as discrete signals. Second, because the input and output discretized fields have dimensions that depend on the discrete resolution of the numerical simulator, designing a multilevel estimator requires the introduction of grid transfer operators, which may be borrowed from multigrid methods [6, 7, 26, 55]. These considerations raise crucial questions about the effect of grid transfer operators on the different scales (or, equivalently, frequencies) of the discretized fields (or signals) that are transferred between grids of different resolutions, and their impact on the resulting multilevel estimator. We address these important questions that, to the best of our knowledge, have not been previously considered in the literature. In particular, we present a numerical illustration of the effects of grid transfer operators on the variance of the MLMC estimator, based on the spectral decomposition of the estimator’s variance in a Fourier-like basis. This leads us to propose a novel, filtered MLMC (F-MLMC) estimator that mitigates the negative effects of the grid transfer operators on the multilevel estimator. The introduction of filtering is supported by a theoretical spectral analysis of the MLMC and F-MLMC estimators in a simplified setting where the numerical simulators are considered to be linear, symmetric and circulant operators. Finally, the proposed F-MLMC approach is successfully tested on a 2D instance of our motivating example.

The remainder of this paper is organized as follows. Section 2 presents the description of the motivating problem of estimating the normalization coefficients of a diffusion-based covariance operator. This problem will be used as an illustration and test case throughout the paper. Section 3 introduces the MLMC estimator of the expectation of discretized random fields, and illustrates its capabilities and limitations on a one-dimensional (1D) test case of the normalization problem. Following the conclusions of this experiment, an F-MLMC estimator is introduced in section 4 and compared to the unfiltered MLMC estimator on the same 1D test problem. A spectral analysis of the MLMC and F-MLMC estimators is then carried out in section 5 to investigate the effects of grid transfer and filtering operators on their variance, in the specific case of linear, symmetric and circulant numerical simulators. In section 6, we apply the MLMC and F-MLMC estimators to the 2D problem of estimating the normalization coefficients of a two-dimensional (2D), heterogeneous, diffusion-based covariance operator. General conclusions are drawn in section 7, along with prospective avenues for future work.

2 Motivation and problem description

As discussed in the introduction, one area where the estimation of the expectation of discretized random fields arises is covariance modelling, specifically when estimating the intrinsic variances of a diffusion-based covariance operator using a randomization method [58, 59]. This particular problem, which is outlined in this section, will be our motivating example throughout the paper.

Let $u: \mathcal{D} \rightarrow \mathbb{R}$ and $b: \mathcal{D} \rightarrow \mathbb{R}$ be square-integrable functions on the domain $\mathcal{D} \subset \mathbb{R}^d$ where $d \in \{1, 2, 3\}$ is the spatial dimension. We consider numerical solutions of the following elliptic equation, subject to application-dependent boundary conditions (BCs):

$$(I - \nabla \cdot \mathbf{K} \nabla)^m u = b, \quad (1)$$

where m is a positive integer, I is the identity operator, and $\mathbf{K}: \mathcal{D} \rightarrow \mathbb{R}^{d \times d}$ is a symmetric, positive-definite (SPD) tensor field with entries $[K_{ij}]_{i,j=1,\dots,d}$. Equation (1) can be interpreted as a semi-discrete representation of a diffusion equation integrated over m time-steps where the temporal derivative is discretized with a backward Euler (implicit) scheme, the time-step is equal to unity, \mathbf{K} is a diffusivity tensor, and the initial condition is b [56]. If \mathbf{K} is constant then the integral solution on \mathbb{R}^d defines a covariance operator whose kernel is a covariance function from the Matérn class [25, 60].

We assume that the operator in eq. (1) is discretized in space on a (not necessarily structured) grid of n cells. We can then deduce the covariance matrix associated with the numerical solution of eq. (1) as

$$\mathbf{L} := (\mathbf{I} - \mathbf{\Delta})^{-m} \mathbf{W}^{-1}, \quad (2)$$

where $\mathbf{\Delta}$ is the matrix representing a spatial discretization of the differential operator $\nabla \cdot \mathbf{K} \nabla$, and $\mathbf{W} \in \mathbb{R}^{n \times n}$ is an SPD Gram matrix that encodes the geometrical and structural information related to the discrete approximation of the diffusive term on the grid. Specifically, \mathbf{W} is such that $\mathbf{\Delta}$ is self-adjoint with respect to the inner product whose weighting matrix is \mathbf{W} , i.e., $\mathbf{W} \mathbf{\Delta} = \mathbf{\Delta}^T \mathbf{W}$. Consequently, the matrix \mathbf{L} is self-adjoint (symmetric) with respect to the canonical inner product. In the experiments, we consider only a diagonal diffusivity tensor $K_{ij} = K_{ij} \delta_{ij}$ where δ_{ij} is the Kronecker delta. Specifically, we define the diagonal elements according to the relation $K_{ii}(\mathbf{x}) = (2m - d - 2)^{-1} (D_{ii}(\mathbf{x}))^2$ where the elements $[D_{ii}(\mathbf{x})]_{i=1,\dots,d}$ correspond to the directional correlation length-scales at the spatial location \mathbf{x} , and $m > d/2 + 1$ [56, section 3].

The matrix \mathbf{L} is SPD but does not define a covariance matrix with meaningful variances for applications like data assimilation. As such, \mathbf{L} must be normalized by its diagonal so that the desired variances can be applied. Thus, we define the covariance matrix of interest as $\mathbf{B} = \mathbf{\Sigma} \mathbf{\Gamma} \mathbf{L} \mathbf{\Gamma} \mathbf{\Sigma}$, where $\mathbf{\Gamma} = \text{Diag}(\text{diag}(\mathbf{L}))^{-1/2}$ is a normalizing diagonal matrix such that $\text{Diag}(\text{diag}(\mathbf{\Gamma} \mathbf{L} \mathbf{\Gamma})) = \mathbf{I}_n$, and $\mathbf{\Sigma}^2 = \mathbf{\Sigma} \mathbf{\Sigma}$ is the diagonal matrix with entries corresponding to the desired variances, i.e., $\text{diag}(\mathbf{B}) = \text{diag}(\mathbf{\Sigma}^2) = (\sigma_1^2, \dots, \sigma_n^2)$. In these expressions, the operator $\text{diag}(\cdot)$ maps a matrix to the vector consisting of the diagonal elements of that matrix, while the operator $\text{Diag}(\cdot)$ maps a vector to the diagonal matrix whose diagonal consists of the entries of that vector. For large-scale problems, the matrix \mathbf{L} is not assembled, and only applications of \mathbf{L} to vectors are accessible. Thus, its diagonal entries $\text{diag}(\mathbf{L}) = \boldsymbol{\theta} = (\theta_1, \dots, \theta_n)$ are not explicitly stored and need to be determined differently [59]. A direct way would be to recover these by applying \mathbf{L} to the canonical basis vectors of \mathbb{R}^n , i.e., $\theta_k = (\mathbf{L} \mathbf{e}_k)_k$, for $k = 1, \dots, n$. For large n , this approach is not computationally tractable.

An alternative strategy is to approximate $\boldsymbol{\theta}$ by randomization. Taking $m = 2q$ and introducing the factorization $\mathbf{W} = \mathbf{V} \mathbf{V}^T$, then \mathbf{L} can be subsequently factored as $\mathbf{L} = \mathbf{A} \mathbf{A}^T$, where

$$\mathbf{A} := (\mathbf{I} - \mathbf{\Delta})^{-q} (\mathbf{V}^{-1})^T, \quad (3)$$

which, as for \mathbf{L} itself, cannot be explicitly assembled in large-scale applications. This decomposition of \mathbf{L} implies that, for any random vector \mathbf{X} with $\mathbb{E}[\mathbf{X}] = \mathbf{0}_n$ and $\mathbb{E}[\mathbf{X}\mathbf{X}^T] = \mathbf{I}_n$,

$$\boldsymbol{\theta} = \text{diag}(\mathbf{L}) = \text{diag}(\mathbf{A}\mathbb{E}[\mathbf{X}\mathbf{X}^T]\mathbf{A}^T) = \text{diag}(\mathbb{C}[\mathbf{A}\mathbf{X}]) = \mathbb{V}[\mathbf{A}\mathbf{X}] = \mathbb{E}[\mathbf{A}\mathbf{X} \odot \mathbf{A}\mathbf{X}], \quad (4)$$

where \odot denotes the Schur product (a.k.a. the Hadamard or element-wise product).

A classical method for estimating the expectation $\boldsymbol{\theta}$ of the \mathbb{R}^n -valued random vector $\mathbf{Y} := \mathbf{A}\mathbf{X} \odot \mathbf{A}\mathbf{X}$ is through Monte Carlo (MC) random sampling. Given a random M -sample $\mathcal{X} = (\mathbf{X}^{(i)})_{i=0}^M$ of \mathbf{X} , an unbiased estimator $\hat{\boldsymbol{\theta}}$ of $\boldsymbol{\theta}$ is the sample mean

$$\hat{\boldsymbol{\theta}} = \frac{1}{M} \sum_{i=1}^M (\mathbf{A}\mathbf{X}^{(i)}) \odot (\mathbf{A}\mathbf{X}^{(i)}). \quad (5)$$

We remark that the estimator $\hat{\boldsymbol{\theta}}$ only requires M applications of \mathbf{A} to a vector, typically with $M \ll n$ in large-scale applications. Furthermore, by construction, the MC estimator defined by eq. (5) yields non-negative estimates, which is a fundamental requirement for the problem under consideration. Alternative MC estimators have been proposed in the literature for estimating the diagonal of a general (not necessarily symmetric) matrix [1, 27], which do not employ a factored form of the matrix and hence do not guarantee non-negative estimates. In all cases, the MC sample mean estimator is known to converge slowly with respect to the sample size M ; specifically, its root-mean-square error (RMSE) is $\mathcal{O}(M^{-1/2})$ [48]. Here, we investigate the use of the MLMC methodology [18, 19] to improve (in terms of RMSE) the estimation of $\boldsymbol{\theta}$ and hence the efficiency of determining accurate normalization coefficients for defining $\boldsymbol{\Gamma}$.

3 MLMC estimation of the expectation of discretized random fields

In this section, we introduce the MLMC ingredients used in the subsequent spectral analysis, focusing on the estimation of the expectation of discretized random fields. The notations introduced here are then used throughout the remainder of this paper. First, general definitions and notations are introduced, then, grid transfer operators are presented as well as their use in the MLMC expectation estimator for discretized fields. Finally, a 1D illustration showcases the MLMC estimator and its benefits compared to a standard MC estimator.

The MLMC method aims to reduce the variance, or sampling error, of MC estimators by combining samples of different fidelities. In favorable cases, many cheap, low-fidelity samples are used to improve the sampling, while fewer are required at finer and more expensive resolutions to correct the bias. Under certain assumptions, [18, Theorem 1] and [9, Theorem 1] ensure that there exists an allocation of samples on a finite number of levels such that the computational cost of the MLMC estimator decreases at a faster rate as a function of the mean square error (MSE), than that of the crude MC estimator. In practice, MLMC is typically implemented as a sequential algorithm, whose main idea is to start with a limited number of coarse fidelity levels, and add as many finer levels as needed to reach a target MSE, with a prescribed variance/bias balance. In the present work, however, we adopt a multilevel approach that is closer to multifidelity methods. Specifically, a fine, high-fidelity level is fixed (and thus so is the bias), while coarser, low-fidelity levels are considered to reduce the variance, for a prescribed computational budget.

3.1 Preliminary notations and definitions

We first describe the MLMC setting for discretized random fields. Let $\{n_\ell\}_{\ell=0}^L$ be an increasing sequence of positive integers corresponding to the size of $L + 1$ grids. Those grids of different

resolutions define the hierarchy of levels needed for the MLMC approach. Specifically, level 0 corresponds to the coarsest level, while level L is the finest. To each level ℓ , we associate the SPD Gram matrix $\mathbf{W}_\ell = \mathbf{V}_\ell \mathbf{V}_\ell^\top \in \mathbb{R}^{n_\ell \times n_\ell}$ that encodes the structural information related to the approximation of continuous functions as a vector of \mathbb{R}^{n_ℓ} on this specific discrete grid. For each level ℓ , we define the weighted inner product $\langle \cdot, \cdot \rangle_{\mathbf{W}_\ell}$ between elements of \mathbb{R}^{n_ℓ} as

$$\forall \mathbf{u}, \mathbf{v} \in \mathbb{R}^{n_\ell}, \quad \langle \mathbf{u}, \mathbf{v} \rangle_{\mathbf{W}_\ell} = \mathbf{u}^\top \mathbf{W}_\ell \mathbf{v} = \langle \mathbf{V}_\ell^\top \mathbf{u}, \mathbf{V}_\ell^\top \mathbf{v} \rangle_{\mathbf{I}_{n_\ell}}, \quad (6)$$

where $\langle \cdot, \cdot \rangle_{\mathbf{I}_{n_\ell}}$ denotes the canonical (Euclidean) dot product between vectors of \mathbb{R}^{n_ℓ} . The norm induced by $\langle \cdot, \cdot \rangle_{\mathbf{W}_\ell}$ is denoted by $\| \cdot \|_{\mathbf{W}_\ell}$. The inner product space $H_\ell := (\mathbb{R}^{n_\ell}, \langle \cdot, \cdot \rangle_{\mathbf{W}_\ell})$ is a separable Hilbert space.

Let \mathbf{X}_L be the \mathbb{R}^{n_L} -valued random vector corresponding to a discretized random field at discrete resolution n_L . We define abstract numerical models $f_\ell: \mathbb{R}^{n_L} \rightarrow \mathbb{R}^{n_\ell}$ of increasing resolution (fidelity) n_ℓ and hence computational cost. We are interested in estimating the expectation of the output of the finest (highest-fidelity) model, $\mathbb{E}[f_L(\mathbf{X}_L)]$. The MLMC estimator $\hat{\boldsymbol{\mu}}_L^{\text{MLMC}}$ of $\mathbb{E}[f_L(\mathbf{X}_L)]$ using $L + 1$ independent M_ℓ -samples of \mathbf{X}_L , $\{\mathcal{X}_L^{(\ell)} = (\mathbf{X}_L^{(\ell,i)})_{i=1}^{M_\ell}\}_{\ell=0}^L$, is defined as

$$\hat{\boldsymbol{\mu}}_L^{\text{MLMC}} = \frac{1}{M_0} \sum_{i=1}^{M_0} f_0(\mathbf{X}_L^{(0,i)}) + \sum_{\ell=1}^L \frac{1}{M_\ell} \sum_{i=1}^{M_\ell} [f_\ell(\mathbf{X}_L^{(\ell,i)}) - f_{\ell-1}(\mathbf{X}_L^{(\ell,i)})]. \quad (7)$$

However, in many applications, the different fidelity models are defined on grids of different resolutions so that their input and output are vectors of \mathbb{R}^{n_ℓ} , instead of \mathbb{R}^{n_L} as required by the definition of f_ℓ . We denote such abstract numerical models by $\tilde{f}_\ell: \mathbb{R}^{n_\ell} \rightarrow \mathbb{R}^{n_\ell}$, for $\ell = 0, \dots, L$, and we are interested in the expectation of the finest output, $\mathbb{E}[f_L(\mathbf{X}_L)]$.

3.2 Grid transfer operators

Because the models \tilde{f}_ℓ have different domains and codomains depending on the resolution, it is not possible to use the MLMC estimator eq. (7) directly. Grid transfer operators are needed to transfer the inputs and outputs between the coarse grids of resolution n_ℓ , $\ell = 0, \dots, L - 1$, and the finest grid of resolution n_L . In order to ease the spectral analysis presented in this paper, we restrict ourselves to linear grid transfer operators, although in principle non-linear transfer operators may be used.

Operators that transfer a discretized field from a coarse grid onto a finer grid are classically referred to as prolongation operators. We denote by $P_\ell^{\ell'}: \mathbb{R}^{n_\ell} \rightarrow \mathbb{R}^{n_{\ell'}}$ the prolongation operator from level ℓ to a finer level $\ell' > \ell$ (i.e., with $n_{\ell'} > n_\ell$). For linear operators, we may identify $P_\ell^{\ell'}$ with the matrix $\mathbf{P}_\ell^{\ell'} \in \mathbb{R}^{n_{\ell'} \times n_\ell}$ such that $P_\ell^{\ell'}(\mathbf{x}_\ell) = \mathbf{P}_\ell^{\ell'} \mathbf{x}_\ell$ for any $\mathbf{x}_\ell \in \mathbb{R}^{n_\ell}$. Besides, so-called restriction operators $R_\ell^{\ell'}: \mathbb{R}^{n_{\ell'}} \rightarrow \mathbb{R}^{n_\ell}$ are used to perform the “reverse” operation of transferring discretized fields defined on level ℓ' to a coarser level $\ell < \ell'$. Again, a linear restriction operator $R_\ell^{\ell'}$ may be identified with the appropriate matrix $\mathbf{R}_\ell^{\ell'} \in \mathbb{R}^{n_\ell \times n_{\ell'}}$. We may now define f_ℓ from \tilde{f}_ℓ as

$$f_\ell = P_\ell^L \circ \tilde{f}_\ell \circ R_\ell^L, \quad (8)$$

for $\ell = 0, \dots, L$, so that the MLMC expression eq. (7) can be applied. These numerical models involve transfer operators between a given level and the finest level L . In practice, these operators may be defined from transfer operators between successive levels, as

$$\mathbf{P}_\ell^L := \mathbf{P}_{L-1}^L \cdots \mathbf{P}_{\ell+1}^{\ell+2} \mathbf{P}_\ell^{\ell+1} \text{ and } \mathbf{R}_\ell^L := \mathbf{R}_{\ell+1}^L \cdots \mathbf{R}_{L-1}^{L-2} \mathbf{R}_L^{L-1}, \quad \forall \ell = 0, \dots, L - 1, \quad (9)$$

and $\mathbf{R}_L^L = \mathbf{P}_L^L = \mathbf{I}_{n_L}$, so that $\tilde{f}_L = f_L$.

3.3 The MLMC estimator

Considering a separable Hilbert space H equipped with the inner product $\langle \cdot, \cdot \rangle_H$ and induced norm $\| \cdot \|_H$, the space of second-order H -valued random variables,

$$L^2(\Omega, H) := \{ \xi : \Omega \rightarrow H \mid \int_{\Omega} \|\xi(\omega)\|_H^2 d\mathbb{P}(\omega) < +\infty \}, \quad (10)$$

is a Hilbert space when equipped with the inner product $\langle \cdot, \cdot \rangle_{L^2(\Omega, H)}$ defined as

$$\forall \xi, \eta \in L^2(\Omega, H), \quad \langle \xi, \eta \rangle_{L^2(\Omega, H)} := \int_{\Omega} \langle \xi(\omega), \eta(\omega) \rangle_H d\mathbb{P}(\omega). \quad (11)$$

The induced norm is denoted by $\| \cdot \|_{L^2(\Omega, H)}$, and, for convenience, we will from now on use the shorthand notation $\| \cdot \|_{L^2(\Omega, H)} = \mathbb{E}[\| \cdot \|_H^2]^{1/2}$. In this paper, we are particularly interested in the spaces $L^2(\Omega, H_\ell)$, for $\ell = 0, \dots, L$, with H_ℓ defined as in section 3.1. In what follows, we assume that $\mathbf{X}_L \in L^2(\Omega, H_L)$ and that, for any $\mathbf{X} \in L^2(\Omega, H_\ell)$,

- $\tilde{f}_\ell(\mathbf{X}) \in L^2(\Omega, H_\ell)$, for $\ell = 0, \dots, L$;
- $P_{\ell-1}^\ell(\mathbf{X}) \in L^2(\Omega, H_\ell)$, for $\ell = 1, \dots, L$;
- $R_{\ell+1}^\ell(\mathbf{X}) \in L^2(\Omega, H_\ell)$, for $\ell = 0, \dots, L-1$.

It follows that $\mathbf{Y}_\ell := f_\ell(\mathbf{X}_L) \in L^2(\Omega, H_\ell)$ for $\ell = 0, \dots, L$. A convergence analysis of the MLMC method in such Hilbert spaces was proposed in [2], from which we reuse here certain definitions and properties.

In particular, we are interested in this work in the normwise MSE of the MLMC estimator with respect to the exact expectation $\boldsymbol{\mu}$, defined by

$$\text{MSE}(\hat{\boldsymbol{\mu}}_L^{\text{MLMC}}, \boldsymbol{\mu}) := \|\hat{\boldsymbol{\mu}}_L^{\text{MLMC}} - \boldsymbol{\mu}\|_{L^2(\Omega, H_L)}^2. \quad (12)$$

As shown in [2, Theorem 3.1]), the MSE admits the decomposition

$$\text{MSE}(\hat{\boldsymbol{\mu}}_L^{\text{MLMC}}, \boldsymbol{\mu}) = \mathcal{V}(\hat{\boldsymbol{\mu}}_L^{\text{MLMC}}) + \|\mathbb{E}[\mathbf{Y}_L] - \boldsymbol{\mu}\|_{\mathbf{W}_L}^2, \quad (13)$$

where

$$\forall \mathbf{Y} \in L^2(\Omega, H_L), \quad \mathcal{V}(\mathbf{Y}) := \|\mathbf{Y} - \mathbb{E}[\mathbf{Y}]\|_{L^2(\Omega, H_L)}^2 = \mathbb{E}[\|\mathbf{Y}\|_{\mathbf{W}_L}^2] - \|\mathbb{E}[\mathbf{Y}]\|_{\mathbf{W}_L}^2. \quad (14)$$

The first term in eq. (13) is referred to as the variance of the multilevel estimator, while the second term corresponds to the squared bias. We note that the multilevel estimator is unbiased with respect to the expectation of the output at the finest level $\boldsymbol{\mu} = \mathbb{E}[\mathbf{Y}_L]$. Furthermore, the variance part of the MSE, $\mathcal{V}(\hat{\boldsymbol{\mu}}_L^{\text{MLMC}})$, can be further decomposed level-wise into

$$\mathcal{V}(\hat{\boldsymbol{\mu}}_L^{\text{MLMC}}) = \frac{1}{M_0} \mathcal{V}(\mathbf{Y}_0) + \sum_{\ell=1}^L \frac{1}{M_\ell} \mathcal{V}(\mathbf{Y}_\ell - \mathbf{Y}_{\ell-1}). \quad (15)$$

3.4 1D illustration

The variance estimation problem described in section 2 is considered here in a 1D setting. We consider cell-centered discretizations of the diffusion operator on the domain $\mathcal{D} := [0, 1]$, with periodic boundary conditions. Specifically, we consider uniform grids composed of n_ℓ cells of size n_ℓ^{-1} , with the associated Gram matrices $\mathbf{W}_\ell = n_\ell^{-1} \mathbf{I}_{n_\ell}$, corresponding to a piecewise constant approximation of the solution. It follows immediately that $\mathbf{V}_\ell = n_\ell^{-1/2} \mathbf{I}_{n_\ell} = \mathbf{W}_\ell^{1/2}$. We define hierarchies of different depth, corresponding to $L \in \{0, \dots, 5\}$, with a fixed finest discretization corresponding to $n_L = 512$. For $\ell = 0, \dots, L-1$, a constant refinement factor $n_{\ell+1}/n_\ell = 2$ is defined, so that $n_\ell = 2^{\ell-L} n_L$. The inter-level prolongation and restriction operators are defined as

$$\mathbf{P}_{\ell-1}^\ell := \begin{bmatrix} 1 & & & \\ & 1 & & \\ & & 1 & \\ & & & \ddots \end{bmatrix} \in \mathbb{R}^{n_\ell \times n_{\ell-1}}, \quad \mathbf{R}_\ell^{\ell-1} := \mathbf{V}_{\ell-1}^{-1} (\mathbf{P}_{\ell-1}^\ell)^\top \mathbf{V}_\ell = \frac{1}{\sqrt{2}} (\mathbf{P}_{\ell-1}^\ell)^\top, \quad (16)$$

respectively, and grid transfer operators between an arbitrary level and the finest level are defined as in eq. (9). This particular choice of grid transfer operators implies that

$$\forall \mathbf{x}_\ell \in \mathbb{R}^{n_\ell}, \|\mathbf{P}_\ell^{\ell'} \mathbf{x}_\ell\|_{\mathbf{W}_{\ell'}} = \|\mathbf{x}_\ell\|_{\mathbf{W}_\ell}, \quad \text{and } \forall \mathbf{X}_{\ell'} \sim \mathcal{N}(\mathbf{0}_{n_{\ell'}}, \mathbf{I}_{n_{\ell'}}), \mathbf{R}_{\ell'}^\ell \mathbf{X}_{\ell'} \sim \mathcal{N}(\mathbf{0}_{n_\ell}, \mathbf{I}_{n_\ell}), \quad (17)$$

for $\ell' > \ell$. Further detail on the motivation for this choice is given in appendix A.

The diffusion tensor field \mathbf{K} (which actually reduces to a scalar field in 1D) is taken to be constant, by setting $D_{11}(\mathbf{x}) = D$ for all $\mathbf{x} \in \mathcal{D}$ (see section 2). The scalar value $D \in \mathbb{R}$ will be referred to as the length-scale and, unless stated otherwise, it will be set to $D = 0.06 \approx 30n_L^{-1}$. Furthermore, we choose a fixed value of $m = 10$, implying that $q = 5$. As described in section 2, the statistic of interest is $\mathbb{E}[f_L(\mathbf{X}_L)] = \mathbb{E}[(\mathbf{A}_L \mathbf{X}_L) \odot (\mathbf{A}_L \mathbf{X}_L)]$, and where \mathbf{X}_L is a standard normal random vector, i.e., $\mathbf{X}_L \sim \mathcal{N}(\mathbf{0}_{n_L}, \mathbf{I}_{n_L})$. The abstract numerical models f_ℓ are defined by eq. (8), with $\tilde{f}_\ell: \mathbf{X}_\ell \mapsto (\mathbf{A}_\ell \mathbf{X}_\ell) \odot (\mathbf{A}_\ell \mathbf{X}_\ell)$, and \mathbf{A}_ℓ defined as in eq. (3) on the appropriate grid of level ℓ . For this experiment, we rely on the optimal sample allocation that minimizes, for a given computational budget η , the variance of the multilevel estimator [41],

$$M_\ell = \left[\frac{\eta}{\mathcal{S}_L} \sqrt{\frac{\mathcal{V}_\ell}{\mathcal{C}_\ell + \mathcal{C}_{\ell-1}}} \right]^+, \quad \mathcal{V}_\ell := \mathcal{V}(\mathbf{Y}_\ell - \mathbf{Y}_{\ell-1}), \quad \mathcal{S}_L := \sum_{\ell=0}^L \sqrt{\mathcal{V}_\ell (\mathcal{C}_\ell + \mathcal{C}_{\ell-1})}, \quad (18)$$

where \mathcal{C}_ℓ denotes the computational cost of one evaluation of f_ℓ and $[\cdot]^+ := \max(1, [\cdot])$, where $[\cdot]$ denotes the floor function. It should be noted that, by convention, the quantities indexed by $\ell = -1$ vanish, so that $\mathcal{C}_{-1} = 0$ and $\mathcal{V}_0 = \mathcal{V}(\mathbf{Y}_0)$. In addition, we remark that, with eq. (18), the prescribed computational budget η may actually be exceeded by an additional cost lower than \mathcal{C}_L . However, this extra cost should be negligible provided $\eta \gg \mathcal{C}_L$. In what follows, we assume a linear computational cost model, specifically $\mathcal{C}_\ell = \mathcal{O}(n_\ell)$, consistent with a fixed number of sparse (banded) matrix-vector applications required for the evaluation of f_ℓ . The variances \mathcal{V}_ℓ are estimated in a preprocessing stage with a pilot sample of size 1000, and the multilevel estimation is conducted with a computational budget $\eta = 100\mathcal{C}_L$.

The sample allocation obtained with these parameters and the total variance of different MLMC estimators is shown in fig. 1a. Instead of requiring 100 fine-grid evaluations like a single-level Monte Carlo estimator, the 2-, 4- and 6-level MLMC estimators only require a few evaluations on the finest level, while more than 900 evaluations are used on the coarsest grid for the 6-level MLMC. The

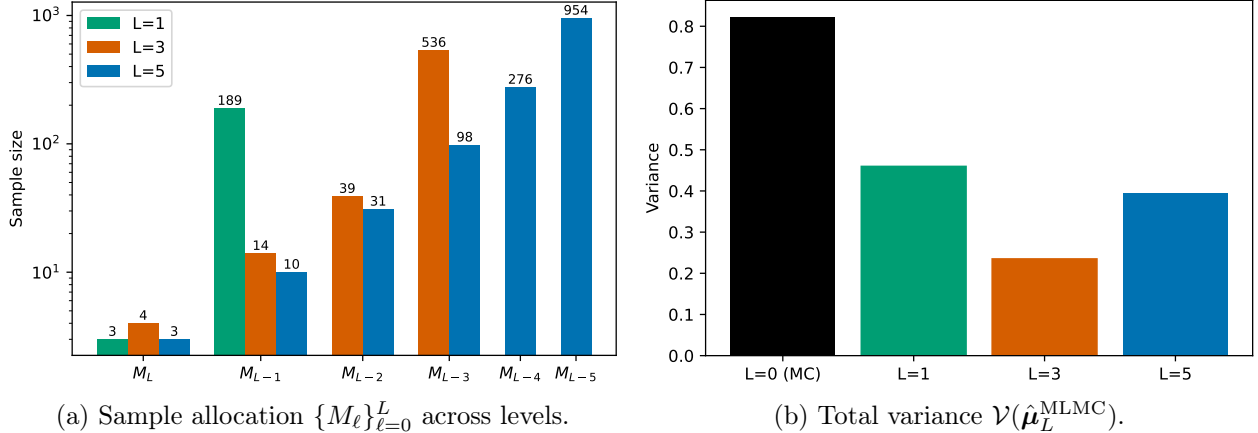


Figure 1: Optimal sample allocation across levels and resulting total variance of the MC estimator ($L = 0$) and different MLMC estimators ($L \in \{1, 3, 5\}$), for the estimation problem described in section 2, with length-scale $D = 0.06$. The finest level L always corresponds to a discretization with $n_L = 512$ cells, and the total budget is set to $\eta = 100C_L$. The variance is estimated from 1000 estimators.

optimal allocation allows for MLMC estimators to reach a lower total variance than the crude MC estimator, as shown in fig. 1b. The minimum variance is achieved with a 4-level MLMC ($L = 3$), with a variance reduction of about 70% compared to MC ($L = 0$). The addition of two coarser levels with 32 and 16 cells, respectively, actually deteriorates the total variance.

The results above suggest that the MLMC estimators in eq. (7) have a lower variance than the single-level MC estimator. However, the variance of the estimator, according to the definition eq. (14), stands here in a normwise (integral) sense, and we cannot infer any information for a specific scale (frequency). In fact, the variance of the estimator associated with a given frequency could provide valuable information for the analysis of multilevel estimators involving discretized fields. In particular, the small-scale (high-frequency) components of a signal on the fine grid cannot be represented on coarser grids.

To study the error at different scales, we decompose the MSE in the Hartley basis [4, 5, 28]. The Hartley basis is a Fourier-like basis, commonly used in circulant embedding techniques for generating stationary Gaussian random fields with prescribed covariance structure [22, 23, 31]. Its main advantage is that it consists of purely real basis vectors, as opposed to the Fourier basis (whose basis vectors are complex), thus easing interpretation and visualization. On level ℓ , the n_ℓ cell-centered Hartley basis vectors $\{\mathbf{h}_k^\ell\}_{k=0}^{n_\ell-1}$ correspond to the columns of the Hartley matrix \mathbf{H}_ℓ with entries

$$(\mathbf{H}_\ell)_{j,k} := \frac{1}{\sqrt{n_\ell}} \left(\cos \frac{2(j + \frac{1}{2})k\pi}{n_\ell} + \sin \frac{2(j + \frac{1}{2})k\pi}{n_\ell} \right), \quad \forall j, k = 0, \dots, n_\ell - 1. \quad (19)$$

The matrices \mathbf{H}_ℓ are orthogonal, i.e., for any $\ell = 0, \dots, L$, $\mathbf{H}_\ell^\top \mathbf{H}_\ell = \mathbf{H}_\ell \mathbf{H}_\ell^\top = \mathbf{I}_{n_\ell}$ (see appendix B). The MSE eq. (12) can thus be decomposed into contributions of the individual Hartley modes,

$$\text{MSE}(\hat{\mu}_L^{\text{MLMC}}, \mu) = \mathbb{E}[\|\hat{\mu}_L^{\text{MLMC}} - \mu\|_{\mathbf{W}_L}^2] = \mathbb{E}[\|\mathbf{H}_L^\top \mathbf{W}_L^{1/2} (\hat{\mu}_L^{\text{MLMC}} - \mu)\|_{\mathbf{I}_{n_L}}^2], \quad (20)$$

which, exploiting the linearity of the expectation operator and the fact that $\mathbf{W}_L = n_L^{-1} \mathbf{I}_{n_L}$, may be

compactly written as

$$\text{MSE}(\hat{\boldsymbol{\mu}}_L^{\text{MLMC}}, \boldsymbol{\mu}) = \|\boldsymbol{\nu}\|_1 := \sum_{k=0}^{n_L-1} \nu_k, \quad \nu_k := n_L^{-1} \mathbb{E}[(\mathbf{h}_k^L)^T (\hat{\boldsymbol{\mu}}_L^{\text{MLMC}} - \boldsymbol{\mu})^2], \quad (21)$$

where $\boldsymbol{\nu} = (\nu_k)_{k=0}^{n_L-1}$ denotes the spectral MSE. In what follows, we take $\boldsymbol{\mu} = \mathbb{E}[\mathbf{Y}_L]$ as a reference, so that the MSE coincides with the variance $\mathcal{V}(\hat{\boldsymbol{\mu}}_L^{\text{MLMC}})$, and $\nu_k = n_L^{-1} \mathbb{V}[(\mathbf{h}_k^L)^T \hat{\boldsymbol{\mu}}_L^{\text{MLMC}}]$. We thus refer to $\boldsymbol{\nu}$ as the spectral variance of the estimator. Furthermore, we define the cumulative variance, $\boldsymbol{\nu}^{\text{cml}} = (\nu_k^{\text{cml}})_{k=0}^{n_L-1}$, such that $\nu_k^{\text{cml}} = \sum_{k'=0}^k \nu_{k'}$, implying that the total variance is given by $\nu_{n_L-1}^{\text{cml}} = \|\boldsymbol{\nu}\|_1$.

In fig. 2, we plot the spectral variance $\boldsymbol{\nu}$, as well as the corresponding cumulative variance $\boldsymbol{\nu}^{\text{cml}}$, associated with the 2-, 4- and 6-level MLMC estimators ($L \in \{1, 3, 5\}$) and with the single-level MC estimator ($L = 0$), for the estimation problem described in section 2, with length-scale $D = 0.06$. Note that, in this and the following figures, the Hartley basis vectors $\{\mathbf{h}_k^\ell\}_{k=0}^{n_\ell-1}$ are reordered by increasing representable frequency (see appendix C). Figure 2a shows that, for the single-level MC estimator, most of the error arises from the first Hartley modes, which are associated with the large scales, or low frequencies, of the discretized field. This is confirmed in fig. 2b, where the cumulative variance of the MC estimator rapidly increases before reaching a plateau, showing that the variance is concentrated on the first few modes. The spectral variances of the MLMC estimators exhibit a similar behavior, but its decay in the high frequencies is less pronounced. For the 2-level MLMC estimator, the spectral variance starts with a similar decay as that of the MC estimator in the low frequencies, before increasing again in the high frequencies. Nevertheless, the variance is still concentrated on the first few modes, and the low-frequency components of the spectral variance are lower than those of the single-level MC estimator. This translates into a lower plateau reached by the cumulative variance, as shown in Figure 2b. Moreover, the variance increase in the high-frequencies translates into a noticeable increase in the cumulative variance in the last few Hartley modes, which, in turn, results in a non-negligible increase in the total variance. As more levels are added, the spectral variance significantly deteriorates in the high-frequencies. While for the 4-level MLMC estimator, this deterioration is compensated by a lower variance in the low frequencies, this is no longer the case for the 6-level MLMC estimator, whose cumulative variance eventually gets larger than that of the 4-level MLMC estimator, thus resulting in a larger total variance, as already evidenced in fig. 1.

It should be noted that the length-scale $D = 0.06$ used for the experiments presented above induces output fields mostly composed of large scales (low frequencies). Decreasing its value increases the frequencies of the output field, thus introducing smaller scales. Figure 3 shows the spectral and cumulative variance of the MC and MLMC estimators for a reduced length-scale $D = 0.01 \approx 5n_L^{-1}$. We observe that the decay of the spectral variance of the MC estimator as the frequency increases is slower than for $D = 0.06$, so that the variance is concentrated on a wider low-frequency range. For the multilevel estimators, we see that the significant deterioration of the variance in the high-frequencies is no longer compensated by a better estimation in the low frequencies, except for the 2-level estimator, which remains slightly better than the single-level estimator in terms of total variance.

4 The filtered MLMC method

The spectral variance of the MLMC estimator for the 1D variance estimation problem shows a significant deterioration of the variance in the high frequencies. Inspired by multigrid methods [7,

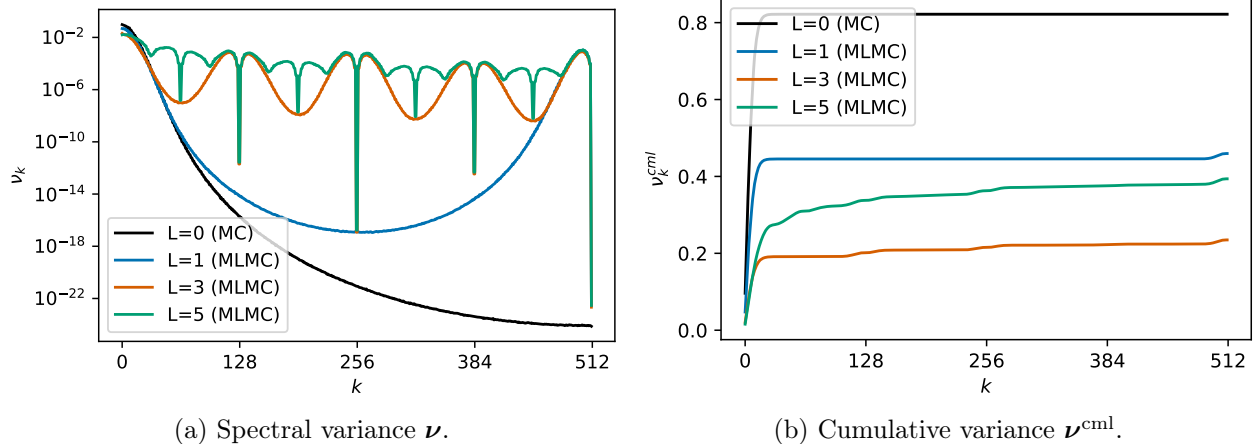


Figure 2: Spectral and cumulative variance of the MC estimator ($L = 0$) and different MLMC estimators ($L \in \{1, 3, 5\}$), for the estimation problem described in section 2, with length-scale $D = 0.06$. The finest level L always corresponds to a discretization with $n_L = 512$ cells, and the total budget is set to $\eta = 100C_L$. The variance is estimated from 1000 estimators.

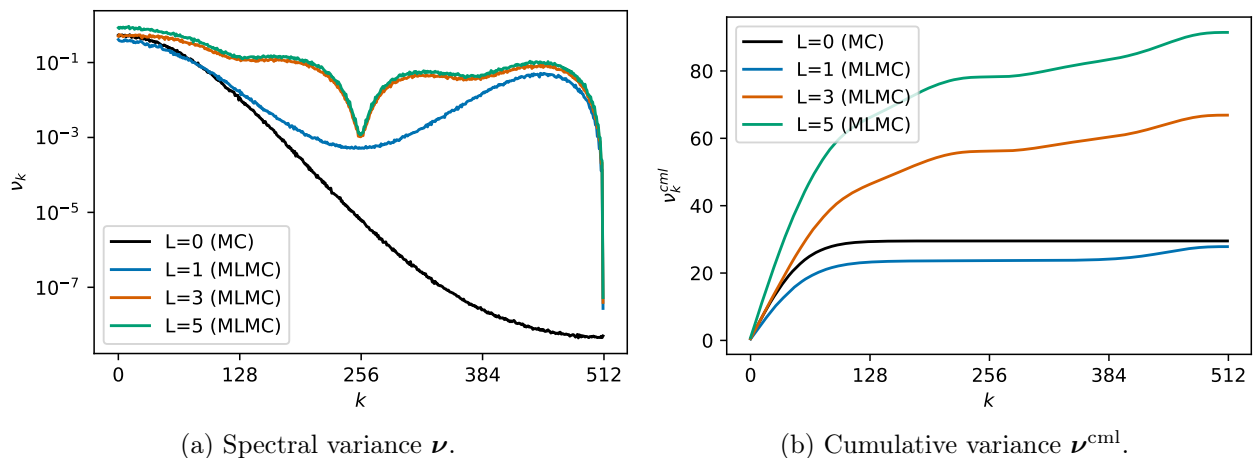


Figure 3: Same as fig. 2 but with length-scale $D = 0.01$.

[55, 61], we propose an improvement of the MLMC estimator for discretized random fields by adding pre- and post-filtering (or, in multigrid terminology, smoothing). The objective is to filter out the smaller scales, which cannot be represented on the coarse grids, before using a restriction operator and after using a prolongation operator.

4.1 Filtered grid transfer operators

Filtering the small-scale components out of a signal on level ℓ is achieved using a low-pass filtering operator $S_\ell: \mathbb{R}^{n_\ell} \rightarrow \mathbb{R}^{n_\ell}$. In what follows, we resort to linear filtering operators S_ℓ , which can thus be identified with matrices \mathbf{S}_ℓ . Filtered grid transfer operators \bar{P}_ℓ^L and \bar{R}_L^ℓ are defined through their corresponding matrices $\bar{\mathbf{P}}_\ell^L$ and $\bar{\mathbf{R}}_L^\ell$ by

$$\bar{\mathbf{P}}_\ell^L := \bar{\mathbf{P}}_{L-1}^L \cdots \bar{\mathbf{P}}_{\ell+1}^{\ell+2} \bar{\mathbf{P}}_\ell^{\ell+1} \quad \text{and} \quad \bar{\mathbf{R}}_L^\ell := \bar{\mathbf{R}}_{\ell+1}^\ell \cdots \bar{\mathbf{R}}_{L-1}^{L-2} \bar{\mathbf{R}}_L^{L-1}, \quad \forall \ell = 0, \dots, L-1 \quad (22)$$

where

$$\bar{\mathbf{R}}_L^{\ell-1} := \mathbf{R}_L^{\ell-1} \mathbf{S}_\ell, \quad \text{and} \quad \bar{\mathbf{P}}_{\ell-1}^\ell := \mathbf{S}_\ell \mathbf{P}_{\ell-1}^\ell \quad \forall \ell = 1, \dots, L, \quad (23)$$

and $\bar{\mathbf{R}}_L^L = \bar{\mathbf{P}}_L^L = \mathbf{I}_{n_L}$. The filtered MLMC estimator, hereafter referred to as the F-MLMC estimator, then reads

$$\hat{\boldsymbol{\mu}}_L^{\text{F-MLMC}} = \frac{1}{M_0} \sum_{i=1}^{M_0} \bar{f}_0(\mathbf{X}_L^{(0,i)}) + \sum_{\ell=1}^L \frac{1}{M_\ell} \sum_{i=1}^{M_\ell} [\bar{f}_\ell(\mathbf{X}_L^{(\ell,i)}) - \bar{f}_{\ell-1}(\mathbf{X}_L^{(\ell,i)})], \quad (24)$$

where $\bar{f}_\ell = \bar{P}_\ell^L \circ \tilde{f}_\ell \circ \bar{R}_L^\ell$, for $\ell = 0, \dots, L$. In what follows, we resort to the second-order Shapiro filter [16, 17, 52] defined as

$$\mathbf{S}_\ell := \frac{1}{4} \begin{bmatrix} 2 & 1 & & 1 \\ 1 & 2 & 1 & \\ & \ddots & \ddots & \ddots \\ & & 1 & 2 & 1 \\ 1 & & & 1 & 2 \end{bmatrix}. \quad (25)$$

With the specific grid transfer operators defined in eq. (16), the operator $\bar{\mathbf{P}}_{\ell-1}^\ell$ corresponds to the linear interpolation operator between the levels $\ell - 1$ and ℓ .

The idea of smoothing highly oscillatory signals within the MLMC framework was also recently exploited in [31], in a setting where the input of the considered simulator is a discretized random field, but where the output is a scalar quantity. Consequently, prolongation operators are not needed, and only restriction operations are required. In fact, because the Cartesian, node-centered, finite element discretization considered in [31] produces nested meshes, the restriction operator reduces to a selection operator, which selects the vector entries associated with the desired nodal unknowns. The pre-smoothing (or pre-filtering) operation proposed in [31] is based on a spectral truncation of the high-frequency components of the input signal, and designed for each MLMC level such that the truncation error matches the discretization error, so that the MLMC properties are best exploited. The combination of this pre-filtering technique with spectral post-filtering, along the lines of [13, section 4.4], may be investigated in future work.

4.2 1D illustration

The 1D variance estimation problem described in section 2 and used in section 3 is again used to illustrate the effects of filtering. The optimal sample allocation, obtained from eq. (18), is reported in fig. 4a for the 6-level ($L = 5$) MLMC and F-MLMC estimators, for a length-scale $D = 0.06$. We observe that the filtered estimator allocates smaller sample sizes to the finer grids than the unfiltered one, while a more than 50% larger sample size is allocated to the coarsest level. This may be explained by the fact that, in the absence of filtering, more effort needs to be made on the finer levels, due to the large high-frequency components of the variance. This change in the optimal allocation has a significant impact on the total variance, as shown by fig. 4b. The F-MLMC estimators achieve a lower total variance than their unfiltered counterpart regardless of the hierarchy, with the 6-level F-MLMC ($L = 5$) achieving the lowest variance. The addition of filters allows the two coarsest grids to reduce the total variance of the estimator further, while the variance of the unfiltered MLMC estimator deteriorates when including these levels.

Figure 5 shows the spectral variance $\boldsymbol{\nu}$ and the cumulative variance $\boldsymbol{\nu}^{\text{cml}}$ of the F-MLMC estimators with different grid hierarchies corresponding to $L \in \{1, \dots, 3\}$. The effects of the filters are especially visible on the spectral variance (fig. 5a), which is significantly reduced, not only in the high frequencies, but also in the lowest ones (i.e., corresponding to the first few Hartley modes), as compared to the unfiltered MLMC (fig. 2a). The reduced error in the high frequencies (small

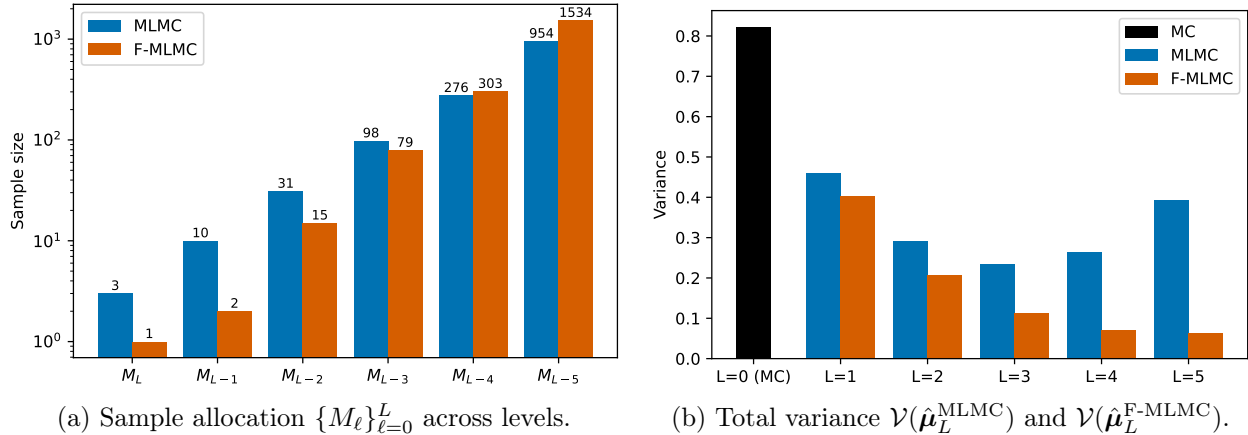


Figure 4: Optimal sample allocation across levels for the 6-level ($L = 5$) MLMC and F-MLMC estimators, and total variance of the MC estimator ($L = 0$) and different MLMC and F-MLMC estimators ($L = 1, \dots, 5$), for the estimation problem described in section 2, with length-scale $D = 0.06$. The finest level L always corresponds to a discretization with $n_L = 512$ cells, and the total budget is set to $\eta = 100C_L$. The variance is estimated from 1000 estimators.

scales) allows the cumulative variance not to be impacted in the last few Hartley modes (fig. 5b), as opposed to the unfiltered MLMC (fig. 2b). Furthermore, the reduced error in the low frequencies (large scales) translates into a lower plateau of the cumulative variance, hence a lower total variance, than for the unfiltered MLMC. Specifically, the addition of filters leads to a 90% reduction in total variance of the F-MLMC estimator compared to the single-level MC estimator, corresponding to a 70% reduction compared to the best, 4-level unfiltered MLMC estimator. The same quantities are plotted in fig. 6 for a length-scale $D = 0.01$. Again, the addition of filters improves the multilevel estimation in both the low and the high frequencies, which in turn benefits the cumulative and thus the total variance. Filtering is here even more beneficial than for $D = 0.06$, in the sense that the F-MLMC estimator has a significantly lower variance than the single-level MC estimator, which the unfiltered MLMC estimator failed to achieve. Specifically, the variance of the 2-level F-MLMC estimator is reduced by about 40% compared to the single-level MC estimator, and that of the 4-level F-MLMC is reduced by more than 50%, while its unfiltered counterpart actually produced a higher variance than the single-level MC estimator.

These experiments highlight that the effect of spurious high frequencies caused by grid transfer operations is detrimental to the MLMC estimator. The addition of pre- and post-filtering operations to mitigate these effects is necessary for the multilevel estimator to reach its full potential.

5 Spectral analysis

In this section, we conduct a spectral analysis of the MLMC estimator eq. (7) and F-MLMC estimator eq. (24) to study more closely the effects of grid transfer operators and filters on the variance of the multilevel estimator at different scales. The analysis is conducted in a 1D setting similar to that of section 3.4, with Gram matrices $\mathbf{W}_\ell = n_\ell^{-1} \mathbf{I}_{n_\ell}$, for $\ell = 0, \dots, L$, corresponding to a cell-centered, piecewise constant approximation of the solution on uniform grids. The setting is further simplified to the case where the numerical simulators are linear, and that their associated matrices are symmetric and circulant.

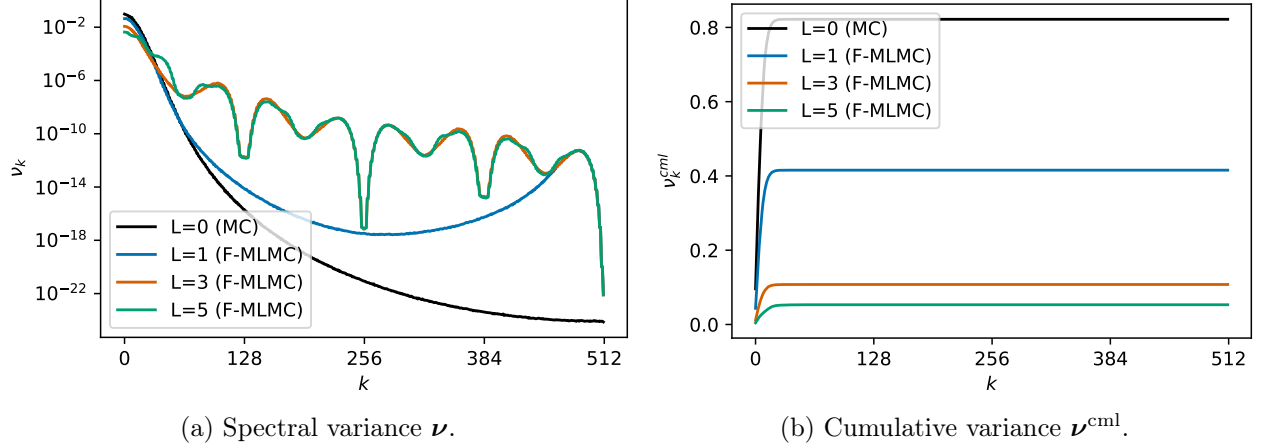


Figure 5: Spectral and cumulative variance of the MC estimator ($L = 0$) and of different F-MLMC estimators ($L \in \{1, 3, 5\}$), for the estimation problem described in section 2, with length-scale $D = 0.06$. The finest level L always corresponds to a discretization with $n_L = 512$ cells, and the total budget is set to $\eta = 100\mathcal{C}_L$. The variance is estimated from 1000 estimators.

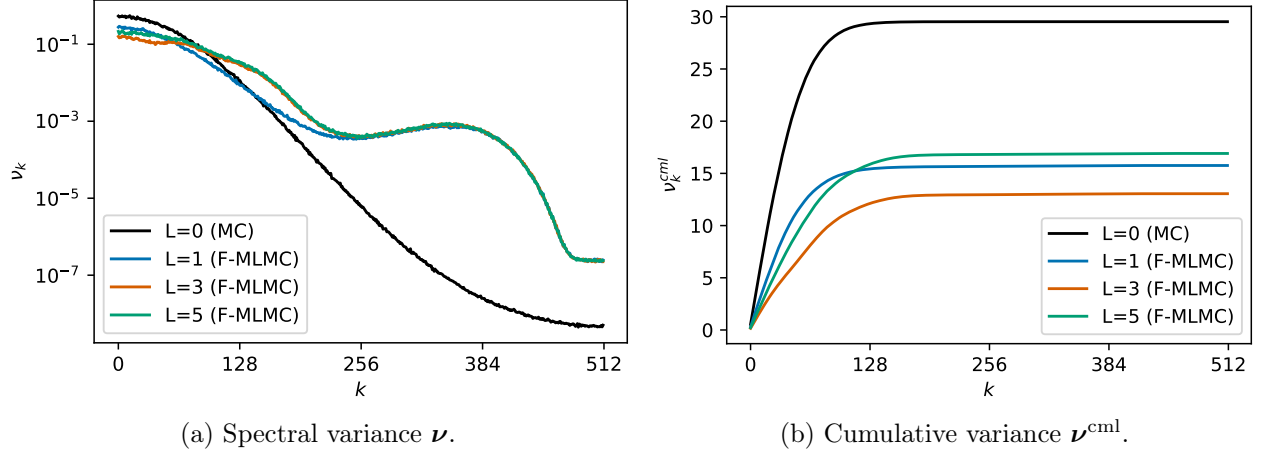


Figure 6: Same as Figure 5 but with length-scale $D = 0.01$.

5.1 MLMC with linear simulators

We consider linear numerical simulators of the form $\tilde{f}_\ell: \mathbf{x}_\ell \mapsto \tilde{\mathbf{F}}_\ell \mathbf{x}_\ell$, where $\tilde{\mathbf{F}}_\ell \in \mathbb{R}^{n_\ell \times n_\ell}$, so that, for a given random vector \mathbf{X}_L corresponding to a discretized random field on the finest level L ,

$$\mathbf{Y}_\ell = \mathbf{F}_\ell \mathbf{X}_L, \quad \mathbf{F}_\ell := \mathbf{P}_\ell^L \tilde{\mathbf{F}}_\ell \mathbf{R}_L^\ell \in \mathbb{R}^{n_L \times n_L}, \quad \forall \ell = 0, \dots, L, \quad (26)$$

with $\mathbf{P}_L^L = \mathbf{R}_L^L = \mathbf{I}_{n_L}$. For now, we make no further assumption on $\tilde{\mathbf{F}}_\ell$. Exploiting the linearity of the simulators, and letting $\mathbf{G} := \mathbb{E}[(\mathbf{X}_L - \mathbb{E}(\mathbf{X}_L))(\mathbf{X}_L - \mathbb{E}(\mathbf{X}_L))^T]$ be the covariance matrix of \mathbf{X}_L , the variance eq. (15) of the multilevel estimator reduces to

$$\mathcal{V}(\hat{\mu}_L^{\text{MLMC}}) = \frac{1}{M_0} \|\mathbf{F}_0 \mathbf{G}^{1/2}\|_{F, \mathbf{W}_L}^2 + \sum_{\ell=1}^L \frac{1}{M_\ell} \|(\mathbf{F}_\ell - \mathbf{F}_{\ell-1}) \mathbf{G}^{1/2}\|_{F, \mathbf{W}_L}^2, \quad (27)$$

where $\|\cdot\|_{F, \mathbf{W}}: \mathbf{M} \mapsto \text{tr}(\mathbf{M}^T \mathbf{W} \mathbf{M})^{1/2}$ denotes the \mathbf{W} -weighted Frobenius norm, for any SPD weighting matrix \mathbf{W} (see appendix D for the derivation of eq. (27)). The variance in eq. (27)

emphasizes that the variance reduction is closely related to the similarity of successive fidelity models. Again, the orthogonality of the Hartley matrix \mathbf{H}_L can be invoked to decompose the variance into contributions of the individual Hartley modes,

$$\mathcal{V}(\hat{\boldsymbol{\mu}}_L^{\text{MLMC}}) = \frac{1}{M_0} \|\mathbf{H}_L^T \mathbf{F}_0 \mathbf{G}^{1/2}\|_{F, \mathbf{W}_L}^2 + \sum_{\ell=1}^L \frac{1}{M_\ell} \|\mathbf{H}_L^T (\mathbf{F}_\ell - \mathbf{F}_{\ell-1}) \mathbf{G}^{1/2}\|_{F, \mathbf{W}_L}^2. \quad (28)$$

5.2 Two-level MLMC with linear, symmetric, circulant simulators

For the remainder of this analysis, we focus on 2-level MLMC estimators ($L = 1$), with n_0 cells on the coarse grid and $n_1 = 2n_0$ cells on the fine grid. Figure 7 depicts the basis vectors \mathbf{h}_k^1 and \mathbf{h}_k^0 of the fine- and coarse-grid Hartley bases, discretized on grids with $n_1 = 16$ and $n_0 = 8$ cells, respectively. These plots highlight that, because of aliasing, the basis vectors exhibit a discrete frequency that is different from their continuous counterpart. Specifically, for $\ell \in \{0, 1\}$, the vectors indexed by k close to 0 or $n_\ell - 1$ are discrete signals with low frequency, while their frequency increases as k tends to $n_\ell/2$.

We now examine the effects of the grid transfer operators on the Hartley basis vectors. Such effects have been studied extensively for multigrid methods [7, 55, 61] using different bases. We succinctly present here results for the specific, cell-centered Hartley basis eq. (19). With the prolongation operator $\mathbf{P} := \mathbf{P}_0^1$ defined in eq. (16), we have (see appendix E)

$$\mathbf{P}\mathbf{h}_k^0 = \sqrt{2}(c_k \mathbf{h}_k^1 - c_{n_0+k} \mathbf{h}_{n_0+k}^1), \quad \forall k = 0, \dots, n_0 - 1, \quad (29)$$

where the coefficients $c_k := \cos(k\pi/(2n_0))$ are strictly decreasing with $k = 0, \dots, 2n_0 - 1$, i.e.,

$$1 = c_0 > c_1 > \dots > (c_{n_0} = 0) > \dots > c_{2n_0-1} > -1. \quad (30)$$

Prolongating a coarse-grid basis vector \mathbf{h}_k^0 , with $k = 0, \dots, n_0 - 1$, produces a (fine-grid) vector consisting of a linear combination of two fine-grid basis vectors \mathbf{h}_k^1 and $\mathbf{h}_{n_0+k}^1$. Figure 7 shows that, for $k \leq n_0/2$, the fine-grid signal \mathbf{h}_k^1 has the same frequency as the original, coarse-grid signal \mathbf{h}_k^0 , while $\mathbf{h}_{n_0+k}^1$ has higher frequency. Conversely, for $k > n_0/2$, the fine-grid signal $\mathbf{h}_{n_0+k}^1$ has the same frequency as the coarse-grid signal \mathbf{h}_k^0 , while \mathbf{h}_k^1 has higher frequency. In both cases, the prolongation of a coarse-grid signal introduces spurious high-frequency (i.e., small-scale) components to the prolonged signal. Fortunately, both \mathbf{h}_k^1 and $\mathbf{h}_{n_0+k}^1$ are damped by a factor which is closer to zero for the spurious, high-frequency signals than for the consistent, low-frequency signals. Specifically, c_k tends to 1 and c_{n_0+k} tends to 0 as k tends to 0, thus damping more severely the spurious, high-frequency signals $\mathbf{h}_{n_0+k}^1$ than the consistent, low-frequency signals \mathbf{h}_k^1 . Conversely, c_k tends to 0 and c_{n_0+k} tends to 1 as k tends to n_0 , thus damping more severely the spurious, high-frequency signals \mathbf{h}_k^1 than the consistent, low-frequency signals $\mathbf{h}_{n_0+k}^1$.

For the restriction operator $\mathbf{R} := \mathbf{R}_1^0$ defined in eq. (16), we have (see appendix F)

$$\mathbf{R}\mathbf{h}_k^1 = c_k \mathbf{h}_k^0, \quad \text{and} \quad \mathbf{R}\mathbf{h}_{n_0+k}^1 = -c_{n_0+k} \mathbf{h}_k^0, \quad \forall k = 0, \dots, n_0 - 1. \quad (31)$$

Restricting a fine-grid basis vector \mathbf{h}_k^1 , with $k = 0, \dots, n_0 - 1$, produces a (coarse-grid) vector proportional to the corresponding coarse-grid basis vector \mathbf{h}_k^0 , specifically, reduced by a factor $c_k \leq 1$. For $n_0/2 < k < n_0$, the restricted signal has lower frequency than the original, fine-grid signal, as illustrates fig. 7. Similarly, restricting a fine-grid basis vector \mathbf{h}_k^1 , with $k = n_0, \dots, 2n_0 - 1$, produces a (coarse-grid) vector proportional to the complementary coarse-grid basis vector $\mathbf{h}_{k-n_0}^0$, specifically reduced by a factor $-c_k < 1$. Again, high-frequency fine-grid signals \mathbf{h}_k^1 corresponding

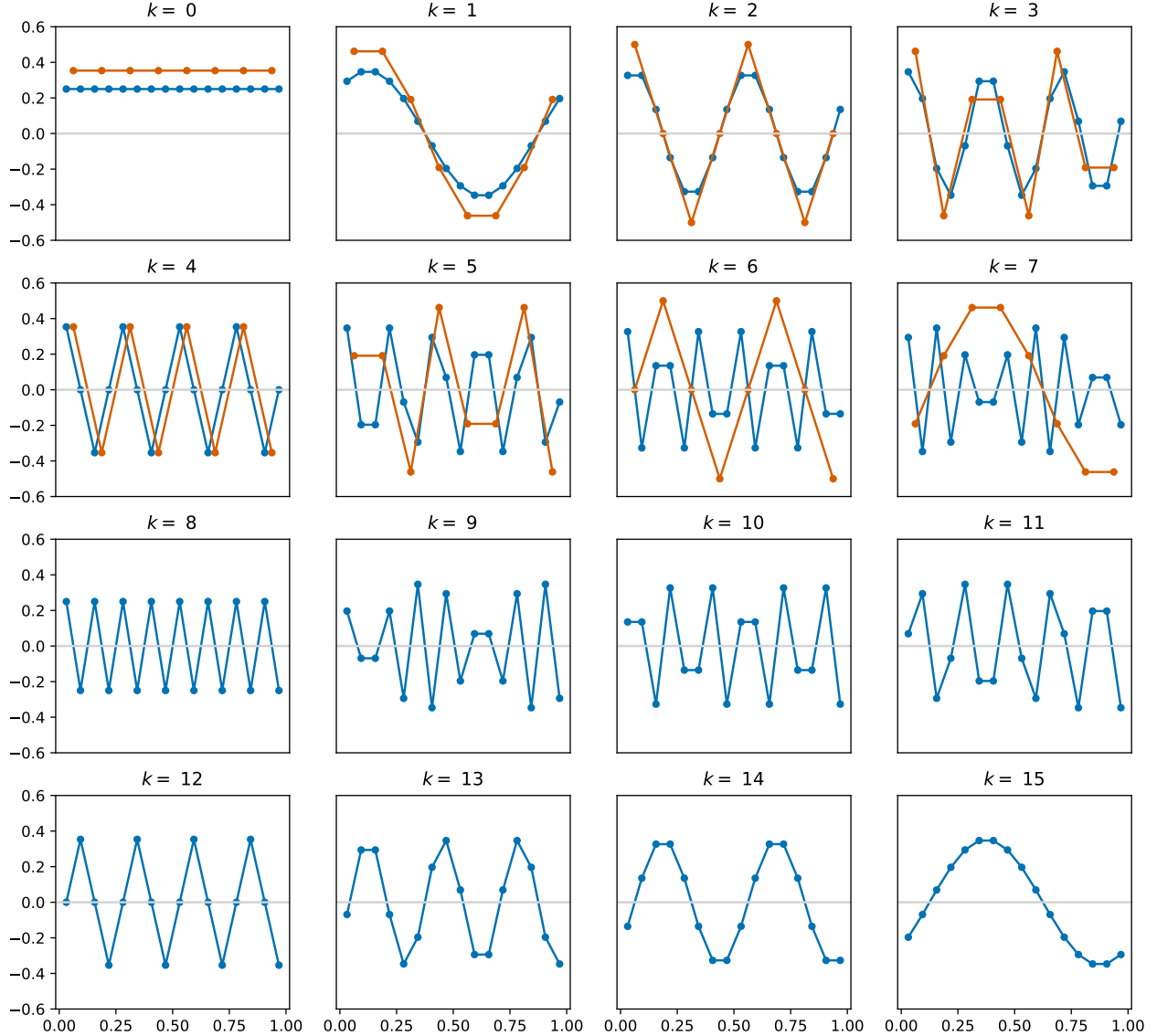


Figure 7: The vectors \mathbf{h}_k^0 (orange) and \mathbf{h}_k^1 (blue) of a coarse-grid Hartley basis \mathbf{H}_0 with $n_0 = 8$ and of a fine-grid Hartley basis with $n_1 = 16$. They are represented on cell-centered grids of size 8 and 16 that discretize the domain $[0, 1]$.

to $n_0 \leq k < 3n_0/2$ are restricted to a signal with lower frequency. In conclusion, high-frequency fine-grid basis vectors that cannot be represented on the coarse grid are thus restricted to lower-frequency signals. Fortunately, such signals are the most damped, since they correspond to ranges of k where c_k is closer to 0.

Remark 1. Denoting $\mathbf{C} := [\text{Diag}(\{c_k\}_{k=0}^{n_0-1}) \quad \text{Diag}(\{-c_{n_0+k}\}_{k=0}^{n_0-1})] \in \mathbb{R}^{n_0 \times 2n_0}$, the identities eqs. (29) and (31) may be compactly recast as

$$\mathbf{P}\mathbf{H}_0 = \sqrt{2}\mathbf{H}_1\mathbf{C}^T, \quad \mathbf{R}\mathbf{H}_1 = \mathbf{H}_0\mathbf{C}, \quad \mathbf{H}_1^T\mathbf{P} = \sqrt{2}\mathbf{C}^T\mathbf{H}_0^T, \quad \mathbf{H}_0^T\mathbf{R} = \mathbf{C}\mathbf{H}_1^T, \quad (32)$$

where the last two identities follow from the first two by exploiting the orthogonality of \mathbf{H}_0 and \mathbf{H}_1 .

We now assume that the operators $\tilde{\mathbf{F}}_\ell$ are symmetric, circulant matrices. Such matrices can be

diagonalized in the Hartley basis [4] (see appendix G for the proof with the cell-centered basis), i.e.,

$$\tilde{\mathbf{F}}_\ell = \mathbf{H}_\ell \mathbf{\Lambda}_\ell \mathbf{H}_\ell^\top, \quad \mathbf{\Lambda}_\ell := \text{Diag}(\{\lambda_k^\ell\}_{k=0}^{n_L-1}), \quad \text{for } \ell \in \{0, 1\}. \quad (33)$$

This property, along with the identities in eq. (32), allows $\mathbf{F}_0 := \mathbf{P}\tilde{\mathbf{F}}_0\mathbf{R} = \mathbf{P}\mathbf{H}_0\mathbf{\Lambda}_0\mathbf{H}_0^\top\mathbf{R}$ to be decomposed as $\mathbf{F}_0 = \mathbf{H}_1\mathbf{M}\mathbf{H}_1^\top$, where $\mathbf{M} := \mathbf{C}^\top\mathbf{\Lambda}_0\mathbf{C} = \begin{bmatrix} \mathbf{M}_{11} & \mathbf{M}_{12} \\ \mathbf{M}_{21} & \mathbf{M}_{22} \end{bmatrix}$, with

$$\mathbf{M}_{11} := \sqrt{2} \text{Diag}(\{c_k^2 \lambda_k^0\}_{k=0}^{n_0-1}), \quad (34)$$

$$\mathbf{M}_{22} := \sqrt{2} \text{Diag}(\{c_{n_0+k}^2 \lambda_k^0\}_{k=0}^{n_0-1}), \quad (35)$$

$$\mathbf{M}_{12} := \sqrt{2} \text{Diag}(\{-c_k c_{n_0+k} \lambda_k^0\}_{k=0}^{n_0-1}) = \mathbf{M}_{21}. \quad (36)$$

As a consequence, eq. (28) becomes

$$\mathcal{V}(\hat{\boldsymbol{\mu}}_1^{\text{MLMC}}) = \frac{1}{M_0} \|\mathbf{M}\mathbf{H}_1^\top \mathbf{G}^{1/2}\|_{F, \mathbf{W}_1}^2 + \frac{1}{M_1} \|(\mathbf{\Lambda}_1 - \mathbf{M})\mathbf{H}_1^\top \mathbf{G}^{1/2}\|_{F, \mathbf{W}_1}^2. \quad (37)$$

To reduce the variance of the correction term in eq. (37), the difference between \mathbf{M} and $\mathbf{\Lambda}_1$ needs to be as small as possible. First, we note that the two off-diagonal blocks \mathbf{M}_{12} and \mathbf{M}_{21} , which are themselves diagonal matrices, contribute to increasing this difference. On the main diagonal, i.e., in the diagonal blocks \mathbf{M}_{11} and \mathbf{M}_{22} , scaled eigenvalues of $\tilde{\mathbf{F}}_0$ appear twice. To compare these diagonal blocks to the eigenvalues of $\tilde{\mathbf{F}}_1$ in $\mathbf{\Lambda}_1$, further assumptions on $\tilde{\mathbf{F}}_0$ are required. We thus introduce the Galerkin coarse-grid operator, which is an algebraic way of constructing the coarse-grid operator $\tilde{\mathbf{F}}_0$ from the fine-grid operator $\tilde{\mathbf{F}}_1$, and which is widely used in multigrid methods and their analysis [55]. Specifically, the Galerkin operator is defined as

$$\tilde{\mathbf{F}}_0 := \frac{1}{2} \mathbf{R}\tilde{\mathbf{F}}_1\mathbf{P} \in \mathbb{R}^{n_0 \times n_0}. \quad (38)$$

This Galerkin operator is the optimal operator in terms of minimizing $\|\tilde{\mathbf{F}}_1 - \mathbf{P}\tilde{\mathbf{F}}_0\mathbf{R}\|_{F, \mathbf{W}_1}^2$ for $\mathbf{W}_1 = n_1^{-1}\mathbf{I}_{n_1}$ and the grid transfer operators defined by eq. (16) (see appendix H). It follows from eqs. (32) and (38) that the Galerkin operator $\tilde{\mathbf{F}}_0$ can be diagonalized in the Hartley basis as $\tilde{\mathbf{F}}_0 = \mathbf{H}_0\mathbf{\Lambda}_0\mathbf{H}_0^\top$ with $\mathbf{\Lambda}_0 = \frac{1}{\sqrt{2}}\mathbf{C}\mathbf{\Lambda}_1\mathbf{C}^\top$. In other words, the eigenvalues $\{\lambda_k^0\}_{k=0}^{n_0-1}$ of the Galerkin operator $\tilde{\mathbf{F}}_0$ can be expressed from the eigenvalues $\{\lambda_k^1\}_{k=0}^{n_1-1}$ of $\tilde{\mathbf{F}}_1$,

$$\lambda_k^0 = \frac{1}{\sqrt{2}} (c_k^2 \lambda_k^1 + c_{n_0+k}^2 \lambda_{n_0+k}^1), \quad \forall k = 0, \dots, n_0 - 1. \quad (39)$$

The resulting blocks of \mathbf{M} then read

$$\mathbf{M}_{11} = \text{Diag}(\{c_k^4 \lambda_k^1 + c_k^2 c_{n_0+k}^2 \lambda_{n_0+k}^1\}_{k=0}^{n_0-1}), \quad (40)$$

$$\mathbf{M}_{22} = \text{Diag}(\{c_{n_0+k}^4 \lambda_{n_0+k}^1 + c_k^2 c_{n_0+k}^2 \lambda_k^1\}_{k=0}^{n_0-1}) = \text{Diag}(\{c_k^4 \lambda_k^1 + c_{k-n_0}^2 c_k^2 \lambda_{k-n_0}^1\}_{k=n_0}^{2n_0-1}), \quad (41)$$

$$\mathbf{M}_{12} = \text{Diag}(\{-c_k^3 c_{n_0+k} \lambda_k^1 - c_k c_{n_0+k}^3 \lambda_{n_0+k}^1\}_{k=0}^{n_0-1}) = \mathbf{M}_{21}. \quad (42)$$

Using elementary trigonometric identities, we remark that $c_{k-n_0} = c_{n_0+k-2n_0} = -c_{n_0+k}$. Therefore, the main diagonal of \mathbf{M} deviates from $\mathbf{\Lambda}_1$ by a multiplicative damping factor $c_k^4 \leq 1$ for $k = 0, \dots, 2n_0 - 1$, on the one hand, and by the addition of a spurious, complementary eigenvalue, though also damped by $c_k^2 c_{n_0+k}^2 < 1$ for $k = 0, \dots, 2n_0 - 1$. The off-diagonal blocks \mathbf{M}_{12} and \mathbf{M}_{21} introduce spurious terms that contribute to the difference $\mathbf{\Lambda}_1 - \mathbf{M}$ and thus increase the variance

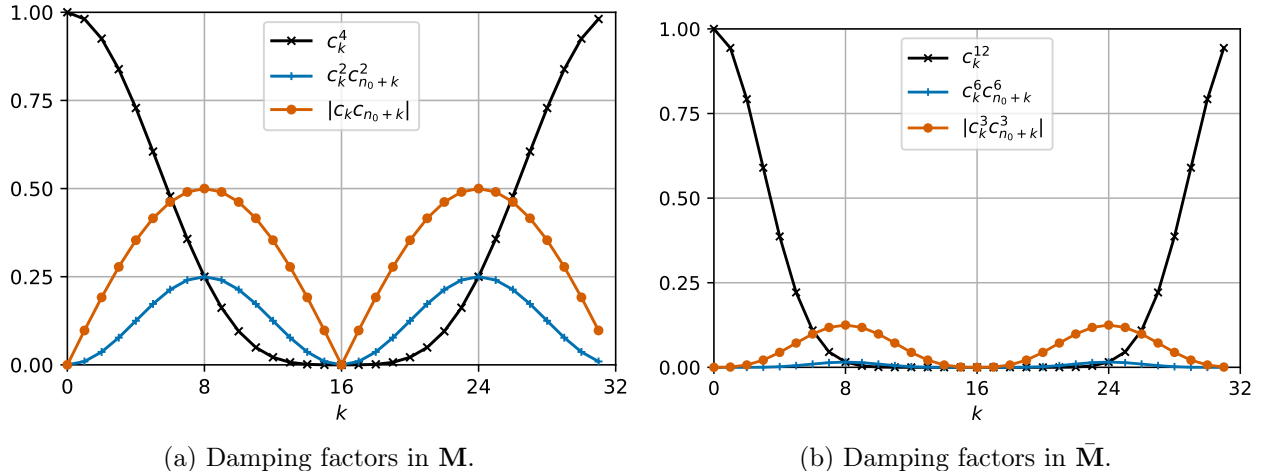


Figure 8: Damping factors of the eigenvalues in \mathbf{M} and $\bar{\mathbf{M}}$ as functions of $k = 0, \dots, n_1 - 1$ with $n_1 = 2n_0 = 32$, when using the Galerkin operator eq. (38). The black curves correspond to the factors of the correct eigenvalues on the main diagonal, while blue curves represent the factors of the spurious eigenvalues. The orange curves correspond to the factors of the off-diagonal blocks.

of the 2-level estimator. Note that, because these terms are to be compared with 0, the comparison with the eigenvalues of the fine-grid operator $\tilde{\mathbf{F}}_1$ are of little interest, which is why we simply consider the damping factors $-\sqrt{2}c_k c_{n_0+k}$ with respect to eigenvalues λ_k^0 of the coarse-grid operator $\tilde{\mathbf{F}}_0$, for $k = 0, \dots, n_0 - 1$, given by eq. (36).

The evolution with $k = 0, \dots, n_1 - 1$ of the three damping factors is presented in fig. 8a. We observe that the eigenvalues λ_k^1 associated with fine, low-frequency Hartley basis vectors, i.e., for k close to 0 and $n_1 - 1$ (see fig. 7), are well-represented on the main diagonal of \mathbf{M} , since $c_k^4 \approx 1$. At the same time, the damping factors $c_k^2 c_{n_0+k}^2$ corresponding to spurious components are close to 0, resulting in small values of the first and last few diagonal entries of the difference $\mathbf{\Lambda}_1 - \mathbf{M}$. In particular, we note that the first entry of \mathbf{M}_{11} exactly matches that of $\mathbf{\Lambda}_1$, i.e., λ_0^1 , because $c_0 = 1$ and $c_{n_0} = 0$. On the other hand, eigenvalues λ_k^1 associated with fine, medium- to high-frequency Hartley basis vectors are severely damped since c_k^4 quickly decreases to 0 as k approaches $n_0 = n_1/2$. Spurious diagonal components are also somewhat damped by a factor $c_k^2 c_{n_0+k}^2$, which is maximal for $k \in \{n_1/4, 3n_1/4\}$. Finally, the spurious, off-diagonal components are damped by a factor $-\sqrt{2}c_k c_{n_0+k}$, which is maximal for $k \in \{n_1/4, 3n_1/4\}$.

5.3 Two-level F-MLMC with linear, symmetric, circulant simulators

We now consider the filtered grid transfer operators defined in section 4.1, $\bar{\mathbf{P}} = \mathbf{S}_1 \mathbf{P}$ and $\bar{\mathbf{R}} = \mathbf{R} \mathbf{S}_1$, where \mathbf{S}_1 denotes the second-order Shapiro filter defined in eq. (25). Similarly to eqs. (29) and (31), it is possible to study the effect the filtered transfer operators on the Hartley basis vectors (see appendix I for the derivations). For the prolongation $\bar{\mathbf{P}}$, we have

$$\bar{\mathbf{P}} \mathbf{h}_k^0 = \sqrt{2}(c_k^3 \mathbf{h}_k^1 - c_{n_0+k}^3 \mathbf{h}_{n_0+k}^1), \quad \forall k = 0, \dots, n_0 - 1. \quad (43)$$

The addition of the Shapiro filter raises the damping factors c_k to the power 3. The prolonged Hartley basis vectors are thus more severely damped than they were without filtering. Again, the most damped fine-grid basis vectors \mathbf{h}_k^1 are those corresponding to k close to $n_0 = n_1/2$, i.e., high-frequency signals. For the restriction operator we have

$$\bar{\mathbf{R}} \mathbf{h}_k^1 = c_k^3 \mathbf{h}_k^0, \quad \text{and} \quad \bar{\mathbf{R}} \mathbf{h}_{n_0+k}^1 = -c_{n_0+k}^3 \mathbf{h}_k^0, \quad \forall k = 0, \dots, n_0 - 1. \quad (44)$$

Similar conclusions can be drawn as for the unfiltered case, but with the damping factors raised to the power of 3, thus increasing the damping, which still affects more strongly the fine-grid, high-frequency signals that cannot be represented on the coarse grid. Similarly to the unfiltered case (see remark 1, identities eqs. (43) and (44) can be recast as

$$\bar{\mathbf{P}}\mathbf{H}_0 = \sqrt{2}\mathbf{H}_1\mathbf{C}_3^T, \quad \bar{\mathbf{R}}\mathbf{H}_1 = \mathbf{H}_0\mathbf{C}_3, \quad \mathbf{H}_1^T\bar{\mathbf{P}} = \sqrt{2}\mathbf{C}_3^T\mathbf{H}_0^T, \quad \mathbf{H}_0^T\bar{\mathbf{R}} = \mathbf{C}_3\mathbf{H}_1^T, \quad (45)$$

where $\mathbf{C}_3 := [\text{Diag}(\{c_k^3\}_{k=0}^{n_0-1}) \quad \text{Diag}(\{-c_{n_0+k}^3\}_{k=0}^{n_0-1})] \in \mathbb{R}^{n_0 \times 2n_0}$.

The impact of filtering on the total variance of the MLMC estimator is now assessed, considering a 2-level MLMC estimator and assuming that $\tilde{\mathbf{F}}_1$ and $\tilde{\mathbf{F}}_0$ are symmetric, circulant matrices. From eqs. (33) and (45), we deduce the decomposition $\tilde{\mathbf{F}}_0 := \bar{\mathbf{P}}\tilde{\mathbf{F}}_0\bar{\mathbf{R}} = \mathbf{H}_1\bar{\mathbf{M}}\mathbf{H}_1^T$, where $\bar{\mathbf{M}} := \begin{bmatrix} \bar{\mathbf{M}}_{11} & \bar{\mathbf{M}}_{12} \\ \bar{\mathbf{M}}_{21} & \bar{\mathbf{M}}_{22} \end{bmatrix}$, with

$$\bar{\mathbf{M}}_{11} = \sqrt{2} \text{Diag}(\{c_k^6 \lambda_k^0\}_{k=0}^{n_0-1}), \quad (46)$$

$$\bar{\mathbf{M}}_{22} = \sqrt{2} \text{Diag}(\{c_{n_0+k}^6 \lambda_k^0\}_{k=0}^{n_0-1}), \quad (47)$$

$$\bar{\mathbf{M}}_{12} = \sqrt{2} \text{Diag}(\{-c_k^3 c_{n_0+k}^3 \lambda_k^0\}_{k=0}^{n_0-1}) = \bar{\mathbf{M}}_{2,1}. \quad (48)$$

Upon replacing \mathbf{F}_0 with its filtered counterpart $\tilde{\mathbf{F}}_0$, eq. (28) can be written as in eq. (37), but with \mathbf{M} replaced by $\bar{\mathbf{M}}$. The sparsity pattern of $\bar{\mathbf{M}}$ is identical to that of \mathbf{M} , and its entries are similar, but with damping factors raised to increased powers. We remark that the off-diagonal blocks $\bar{\mathbf{M}}_{12}$ and $\bar{\mathbf{M}}_{21}$ have entries that are more strongly damped than those of their unfiltered counterparts, \mathbf{M}_{12} and \mathbf{M}_{21} , as can be visualized in fig. 8 (orange plots), which contributes to reducing the off-diagonal entries of $\Lambda_1 - \bar{\mathbf{M}}$ compared to those of $\Lambda_1 - \mathbf{M}$.

To study more closely the diagonal entries of $\bar{\mathbf{M}}$ and compare them to the eigenvalues of $\tilde{\mathbf{F}}_1$ in Λ_1 we resort to the Galerkin operator defined by $\tilde{\mathbf{F}}_0 := \frac{1}{2}\bar{\mathbf{R}}\tilde{\mathbf{F}}_1\bar{\mathbf{P}}$. This definition is inspired by the form of eq. (38), although there is no guarantee of its optimality. Then, from eqs. (33) and (45), it follows that the Galerkin operator $\tilde{\mathbf{F}}_0$ can be diagonalized in the Hartley basis as $\tilde{\mathbf{F}}_0 = \mathbf{H}_0\Lambda_0\mathbf{H}_0^T$ with $\Lambda_0 = \frac{1}{\sqrt{2}}\mathbf{C}_3\Lambda_1\mathbf{C}_3^T$, or, equivalently,

$$\lambda_k^0 = \frac{1}{\sqrt{2}} (c_k^6 \lambda_k^1 + c_{n_0+k}^6 \lambda_{n_0+k}^1), \quad \forall k = 0, \dots, n_0 - 1. \quad (49)$$

The diagonal blocks of $\bar{\mathbf{M}}$ thus become

$$\bar{\mathbf{M}}_{11} = \text{Diag}(\{c_k^{12} \lambda_k^1 + c_{n_0+k}^6 c_k^6 \lambda_{n_0+k}^1\}_{k=0}^{n_0-1}), \quad (50)$$

$$\bar{\mathbf{M}}_{22} = \text{Diag}(\{c_{n_0+k}^{12} \lambda_{n_0+k}^1 + c_{n_0+k}^6 c_k^6 \lambda_k^1\}_{k=0}^{n_0-1}) = \text{Diag}(\{c_k^{12} \lambda_k^1 + c_{k-n_0}^6 c_k^6 \lambda_{k-n_0}^1\}_{k=n_0}^{2n_0-1}). \quad (51)$$

The conclusions are the same as for the diagonal blocks of \mathbf{M} , but with damping factors raised to higher powers. Consequently, the spurious eigenvalues on the main diagonal are damped more strongly than in the unfiltered case, as can be visualized in fig. 8 (blue plots). Moreover, the factors c_k^8 also damp more strongly the consistent eigenvalues compared to the factors c_k^4 of \mathbf{M} , as can be visualized in fig. 8 (black plots). Although the addition of filters induces a certain loss of (mainly high-frequency) information, the spurious signals introduced by the grid transfer operators are significantly reduced. These results suggest that, for filtering to be beneficial, a tradeoff needs to be found between reducing the detrimental effects induced by the grid transfer operators and degrading of the information of the original signal. The second-order Shapiro filters considered in this paper seem to offer a good compromise. Further endeavors to study and improve the filtering process may be pursued in future work.

6 2D application

In this section, we again apply the filtered MLMC estimator to the variance estimation problem described in section 2, but now considering a 2D diffusion operator and using parameter settings more complex than those in the 1D example presented earlier. Specifically, the diffusivity field \mathbf{K} is now specified to be non-uniform, making the variance field also non-uniform. The considered domain is $\mathcal{D} = (0, 1) \times (0, 2) \subset \mathbb{R}^2$. The boundary conditions are chosen periodic along both directions. The 2D diffusivity tensor field \mathbf{K} is chosen to be diagonal and heterogeneous

$$\mathbf{K} = \frac{1}{2m - 4} \begin{bmatrix} D_{11}^2 & 0 \\ 0 & D_{22}^2 \end{bmatrix}, \quad (52)$$

where, for $i = 1, 2$, $D_{ii}: \mathcal{D} \rightarrow \mathbb{R}$ represents a length-scale field in the i -th direction. As previously, we let $m = 2q = 10$. We model $D_{11} = \zeta(\omega_1)$ and $D_{22} = \zeta(\omega_2)$ as two different realizations of a 2D, periodic Gaussian random field ζ over \mathcal{D} of uniform mean μ_ζ , and of quasi-Gaussian covariance structure with uniform variance $\sigma_\zeta^2 = (\mu_\zeta/5)^2 = 0.04\mu_\zeta^2$ and uniform length-scale D_ζ . In the following experiments, two sets of parameters are considered for ζ , namely $(\mu_\zeta = 0.12, D_\zeta = 0.2)$ and $(\mu_\zeta = 0.02, D_\zeta = 0.04)$. The corresponding realizations used in the subsequent experiments are depicted in fig. 9.

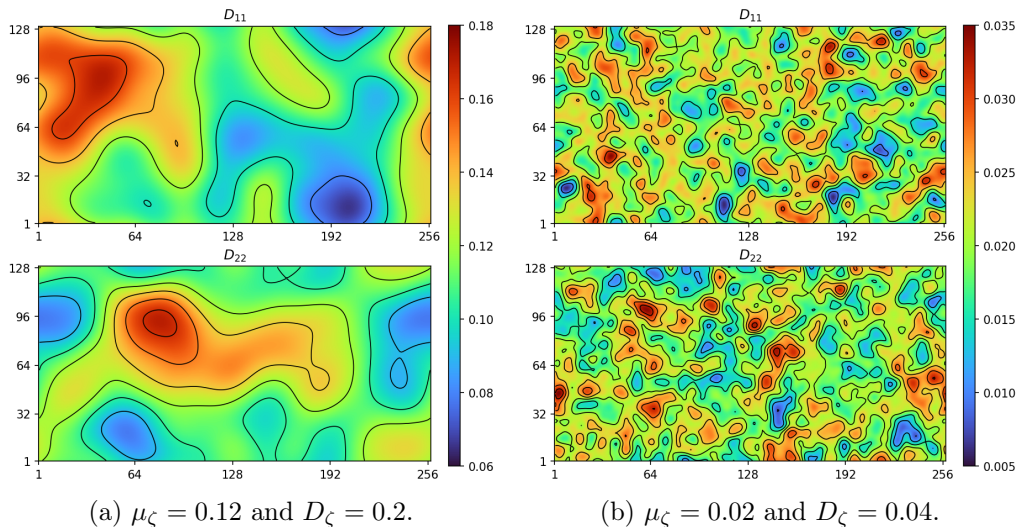


Figure 9: Length-scale fields D_{11} (top) and D_{22} (bottom) used in the reported experiments for the definition of \mathbf{K} in eq. (52), with $\mu_\zeta = 0.12$ and $D_\zeta = 0.2$ (left), and with $\mu_\zeta = 0.02$ and $D_\zeta = 0.04$ (right).

The diffusion operator in eq. (1) is discretized on Cartesian grids of size $n_\ell = n_\ell^x \times n_\ell^y$, with the length-scale fields D_{ij} discretized at edge centers, and the solution discretized at cell centers. The finest grid considered here is composed of $n_L = 256 \times 128$ cells. Three coarser grids are used with a uniform coarsening factor of 4, i.e., $n_{L-1} = 128 \times 64$, $n_{L-2} = 64 \times 32$ and $n_{L-3} = 32 \times 16$. The resulting Gram matrix on level ℓ is given by $\mathbf{W}_\ell = 2n_\ell^{-1}\mathbf{I}_{n_\ell}$. The discrete operators $\mathbf{A}_\ell \in \mathbb{R}^{n_\ell \times n_\ell}$ are designed to apply to and return vectors of size n_ℓ whose entries are associated with cell centers that are sorted by increasing y -coordinate first, then by increasing x -coordinate. In other words, the entry indexed by $k = in_\ell^x + j$ in such vectors is associated with a cell center located at $(x_j, y_i) \in \mathbb{R}^2$, where $x_j := (j + 1/2)/n_\ell^x$ and $y_i := (i + 1/2)/n_\ell^y$, for $j = 1, \dots, n_\ell^x$ and $i = 1, \dots, n_\ell^y$. As in the 1D illustration, we are interested in the multilevel estimation of the fine discretized field

$\boldsymbol{\theta} = \mathbb{E}[(\mathbf{A}_L \mathbf{X}_L) \odot (\mathbf{A}_L \mathbf{X}_L)]$. With the Cartesian ordering of the unknowns described above, the 2D prolongation and restriction operators may be constructed as the Kronecker product of their 1D counterpart, defined in eq. (16), in the x and y directions. The 2D grid transfer operators defined in this manner are then related by $\mathbf{R}_\ell^{\ell-1} = \frac{1}{2}(\mathbf{P}_{\ell-1}^\ell)^\top$, for $\ell = 1, \dots, L$. Likewise, the second-order 2D Shapiro filter is defined as the Kronecker product of two 1D, second-order Shapiro filters defined in eq. (25). The cost model is still considered linear in the number of cells, implying here that one simulator evaluation on level ℓ is as computationally expensive as 4 simulator evaluations on level $\ell - 1$. The baseline is a crude, single-level MC ($L = 0$) computed with a sample of size 100; hence the total budget is $\eta = 100\mathcal{C}_L$.

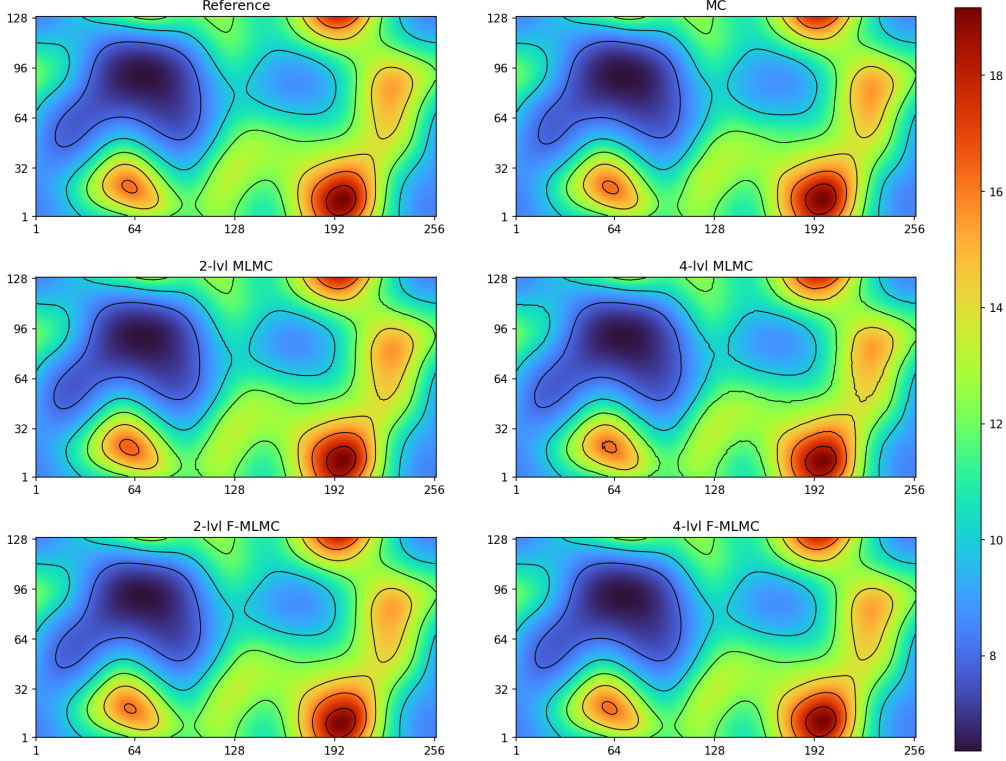


Figure 10: The top-left sub-figure shows the exact discretized field $\boldsymbol{\theta}$ on level L , while the other sub-figures depict the expectation of the single-level MC estimator (top-right), the expectation of the 2- and 4-level MLMC estimators (middle-left and middle-right), and the expectation of the 2- and 4-level F-MLMC estimators (bottom-left and bottom-right). The tensor field \mathbf{K} corresponds to $\mu_\zeta = 0.12$ and $D_\zeta = 0.2$ (fig. 9a). The expectation is approximated from 500 estimators, each constructed with a computational budget $\eta = 100\mathcal{C}_L$.

For a given diffusivity tensor field \mathbf{K} , the exact discretized field $\boldsymbol{\theta}$ on the finest level L is computed explicitly as $\theta_k = (\mathbf{L}\mathbf{e}_k)_k$, for $k = 1, \dots, n_L$, where \mathbf{L} denotes the discrete diffusion operator defined in eq. (2) on level L and \mathbf{e}_k denotes the k -th canonical basis vector of \mathbb{R}^{n_L} . The top-left sub-figure of fig. 10 presents the obtained field $\boldsymbol{\theta}$ for a fixed tensor field \mathbf{K} obtained as described above with parameters $\mu_\zeta = 0.12$ and $D_\zeta = 0.2$. The other sub-figures represent the expectation of the compared estimators, namely the single-level MC estimator, and the 2- and 4-level (F-)MLMC estimators. The expectation is approximated from 500 estimators, each constructed with a computational budget $\eta = 100\mathcal{C}_L$. These figures confirm a key property of the MC and (F-)MLMC estimators, namely that they are unbiased. Indeed, their expectations visually coincide

(up to statistical error due to the estimation) with the reference, i.e., $\mathbb{E}[\hat{\boldsymbol{\theta}}] = \boldsymbol{\theta}$. Consequently, the MSE solely consists of the variance of the estimators.

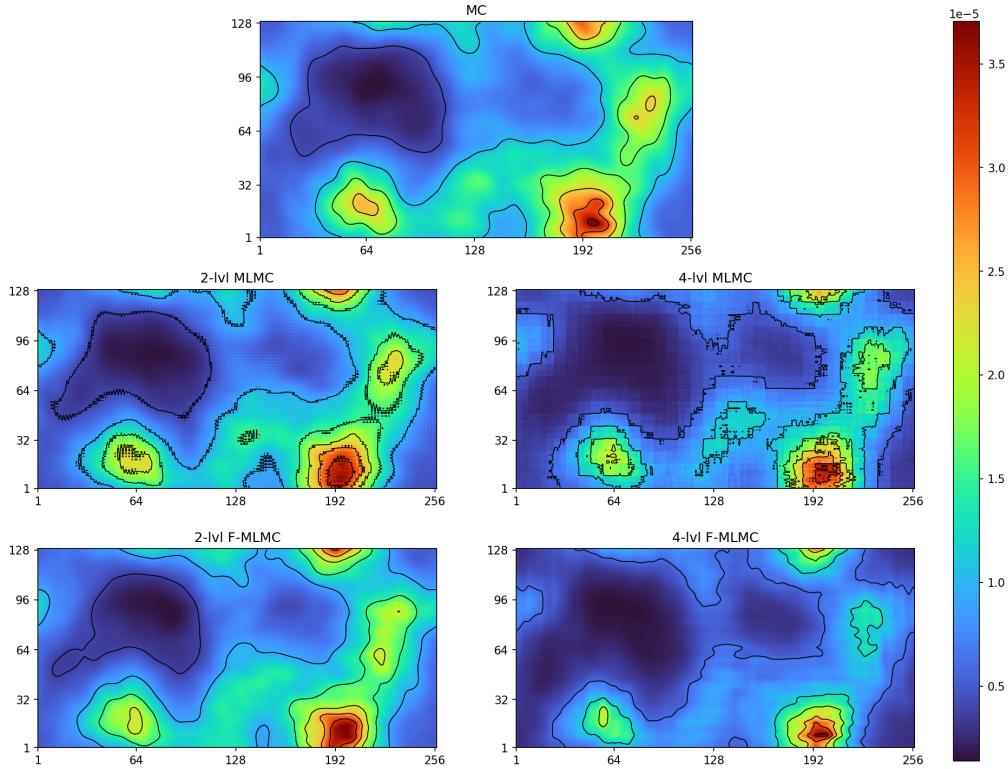


Figure 11: Variance of the MC estimator (top), of the 2- and 4-level MLMC estimators (middle-left and middle-right), and of the 2- and 4-level F-MLMC estimators (bottom-left and bottom-right). The tensor field \mathbf{K} corresponds to $\mu_\zeta = 0.12$ and $D_\zeta = 0.2$ (fig. 9a). The variance is approximated from 500 estimators, each constructed with a computational budget $\eta = 100\mathcal{C}_L$.

Figure 11 shows the variance of the considered estimators. Although the variance of the MLMC estimators (middle row) visually seems lower than that of the MC estimator (top row), we clearly observe high-frequency fluctuations in the variance field, both for the 2-level (left) and the 4-level (right) unfiltered MLMC estimators. These high-frequency components of the variance may have significant consequences on individual estimations of $\boldsymbol{\theta}$. Indeed, while the MLMC estimations will, on average, match the desired field (owing to the unbiasedness of the estimators), individual estimations will be polluted by high-frequency error components because of the large high-frequency components of the variance. The bottom row of fig. 11 demonstrates, at least visually, that the addition of filtering effectively damps these high-frequency components. These observations are confirmed by fig. 12, which shows the spectral decomposition of the variance in the Hartley space, allowing for the visualization of the contribution of each scale (or frequency) to the variance. The Hartley matrix \mathbf{H}_L used to project the 2D variance (discretized) fields onto the Hartley spectral space is defined as the Kronecker product of two 1D Hartley matrices defined in eq. (19). The 2D spectral variance is defined as $\boldsymbol{\nu} = (\nu_k)_{k=0}^{n_L-1} \in \mathbb{R}^{n_L}$, with

$$\nu_k := 2n_L^{-1} \mathbb{E}[(\mathbf{h}_k^L)^T (\hat{\boldsymbol{\theta}}_L^{\text{MLMC}} - \boldsymbol{\theta})^2], \quad k = 0, \dots, n_L - 1, \quad (53)$$

where \mathbf{h}_k^L denotes the k -th column of \mathbf{H}_L . Again, the columns of \mathbf{H}_L are re-ordered so that, in fig. 12, the frequencies in the x and y directions increase along the associated axes, starting from

the lower-left corner, corresponding to low frequencies (large scales). We observe that the variance of the unfiltered MLMC estimators (middle row) clearly exhibits larger high-frequency components than the single-level MC estimator (top row), with values of the same order of magnitude as the low-frequency components. This not only translates into noticeable high-frequency fluctuations of the variance field, as evidenced in fig. 11, but it may also deteriorate the overall variance, as was the case in some instances in the 1D illustration (see section 4.2).

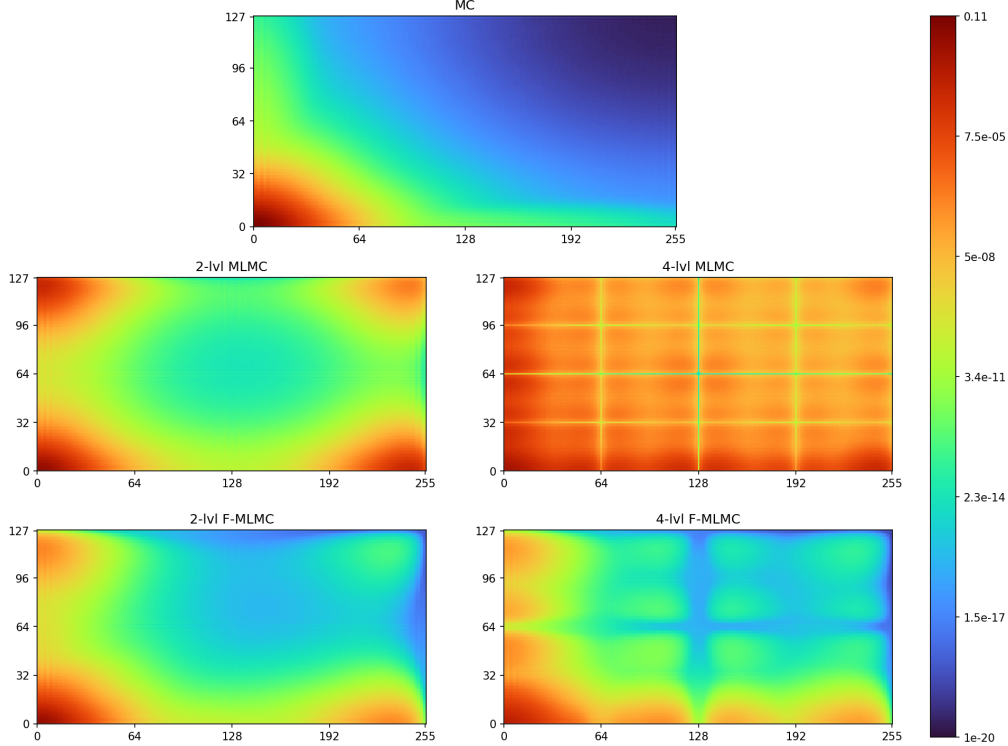
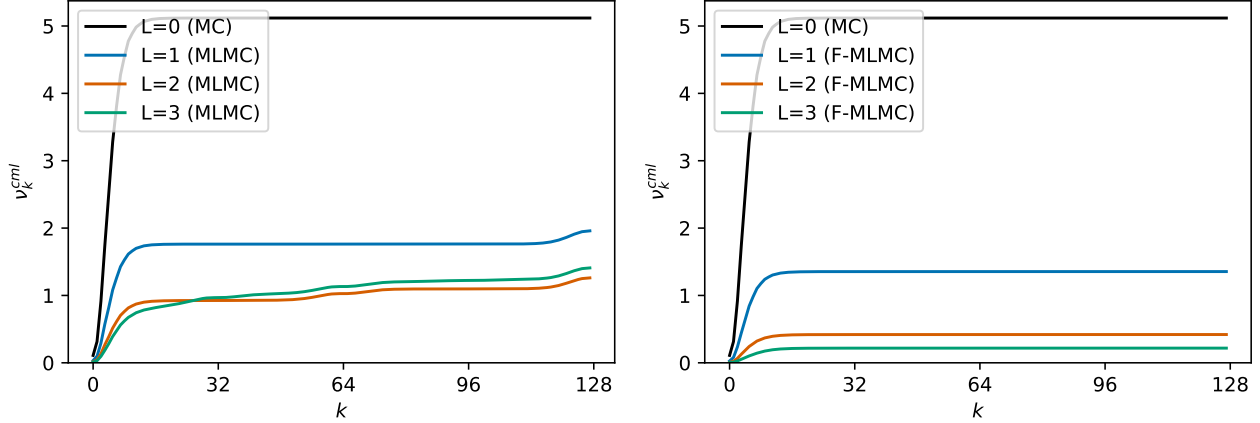


Figure 12: Spectral variance ν of the MC estimator (top), of the 2- and 4-level MLMC estimators (middle-left and middle-right), and of the 2- and 4-level F-MLMC estimators (bottom-left and bottom-right). The tensor field \mathbf{K} corresponds to $\mu_\zeta = 0.12$ and $D_\zeta = 0.2$ (fig. 9a). The variance is approximated from 500 estimators, each constructed with a computational budget $\eta = 100\mathcal{C}_L$.

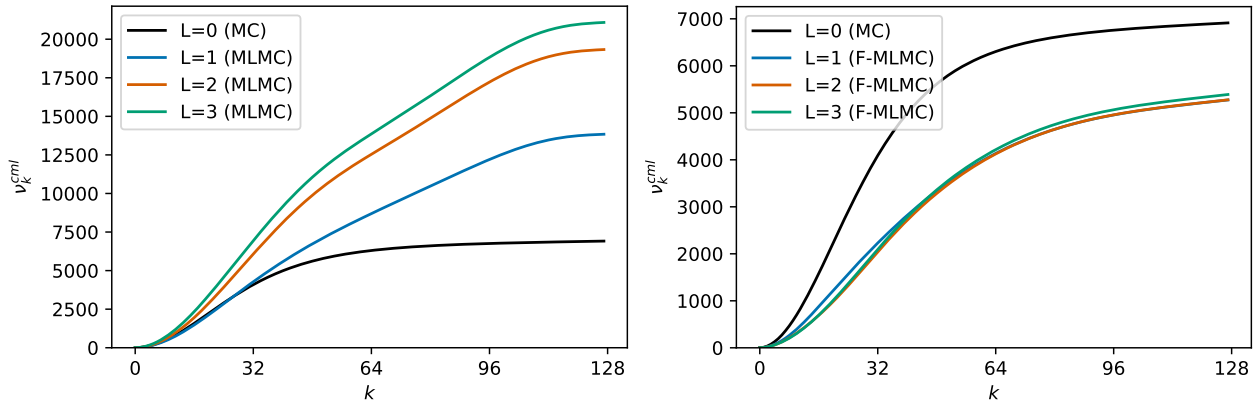
With the Cartesian indexing and the re-ordering of the Hartley basis vectors described earlier, the 2D cumulative variance $\nu^{\text{cml}} = (\nu_k^{\text{cml}})_{k=0}^{n_L^y-1} \in \mathbb{R}^{n_L^y}$ is computed by adding the components of the 2D spectral variance eq. (53) shown in fig. 12 in rectangle patterns starting with the bottom-left corner. Specifically,

$$\nu_k^{\text{cml}} = \sum_{i=0}^k \sum_{j=0}^{2k+1} \nu_{in_L^x+j}, \quad k = 0, \dots, n_L^y - 1. \quad (54)$$

As such, the first components of ν^{cml} represent the cumulative variance associated with the low frequencies (large scales), while the last component $\nu_{n_L^y-1}^{\text{cml}}$ coincides with the total variance of the estimator. Figure 13 presents the cumulative variance of the MLMC and F-MLMC estimators for \mathbf{K} corresponding to $(\mu_\zeta = 0.12, D_\zeta = 0.2)$ and $(\mu_\zeta = 0.02, D_\zeta = 0.04)$. In the first case (fig. 13a), for both the MC, the MLMC and the F-MLMC estimators, most of the variance is concentrated in the lower frequencies. Although the low-frequency contribution to the variance is significantly reduced by the MLMC estimator, a non-negligible contribution of the high frequencies to the variance is



(a) \mathbf{K} with $\mu_\zeta = 0.12$ and $D_\zeta = 0.2$ (fig. 9a).



(b) \mathbf{K} with $\mu_\zeta = 0.02$ and $D_\zeta = 0.04$ (fig. 9b).

Figure 13: Cumulative variance of the MC estimator ($L = 0$) and of different MLMC estimators (left) and F-MLMC estimators (right) with $L \in \{1, 2, 3\}$. The tensor field \mathbf{K} corresponds to $\mu_\zeta = 0.12$ and $D_\zeta = 0.2$ (top), and $\mu_\zeta = 0.02$ and $D_\zeta = 0.04$ (bottom). The variance is approximated from 500 estimators, each constructed with a computational budget $\eta = 100\mathcal{C}_L$.

noticeable. Adding filters reduces the error in the high frequencies, as was observed previously in the spectral decomposition of the variance (fig. 12), but it also reduces the error on the lower frequencies, thus leading to lower total variance. In the second case (fig. 13b), corresponding to a tensor field \mathbf{K} with smaller scales (see fig. 9b), the MLMC estimators deteriorate the variance compared to the crude MC estimator. The addition of a coarser grid ($L = 1$) and the corresponding grid transfer operators induce significant variance in the high-frequency components, leading to an increased total variance. The degradation is all the more pronounced as coarser grids are added ($L = 2$ and $L = 3$). We observe that the addition of filters mitigates these effects and allows the F-MLMC estimators to produce an effective reduction of the variance. The addition of coarser grids ($L = 2$ and $L = 3$) does not bring further improvement, but does not deteriorate the total variance either. The low-frequency (large-scale) components are already well-captured by the two finer grids. This can be explained by the fact that the spectral content of the samples is shifted to higher frequencies. In such a case, a different grid hierarchy, starting from a finer grid, would be more appropriate, although finer discretizations may not always be available or affordable in an operational context. These results are summarized in terms of total variance in fig. 14.

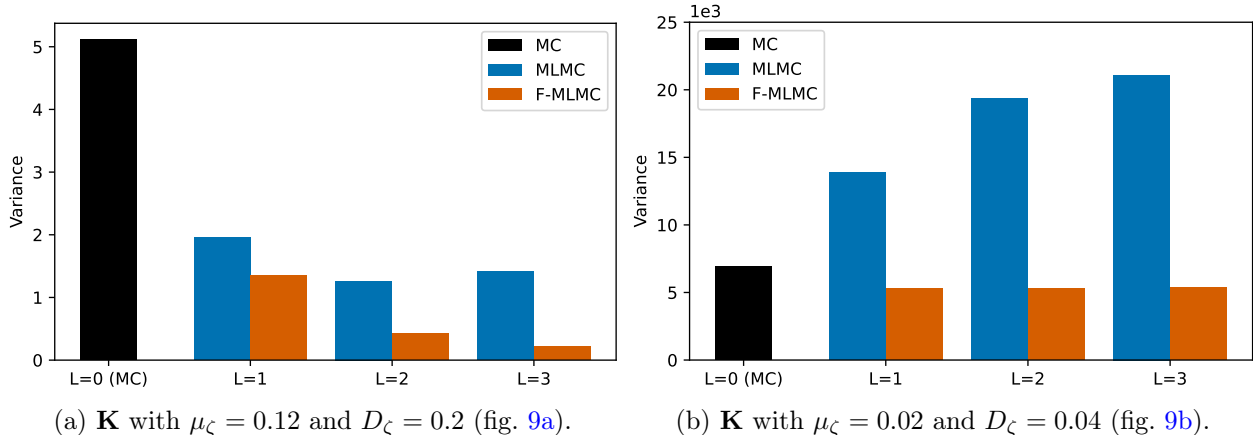


Figure 14: Total variance of the MC estimator ($L = 0$) and of different MLMC estimators and F-MLMC estimators with $L \in \{1, 2, 3\}$. The tensor field \mathbf{K} corresponds to $\mu_\zeta = 0.12$ and $D_\zeta = 0.2$ (left), and $\mu_\zeta = 0.02$ and $D_\zeta = 0.04$ (right). The variance is approximated from 500 estimators, each constructed with a computational budget $\eta = 100\mathcal{C}_L$.

7 Conclusion

In this paper, we focused on the estimation of the expectation of a discretized field using a multilevel, MLMC-like estimator. The different fidelity levels considered are grids of different resolutions, which requires the use of grid transfer operators in the estimator. The resulting MLMC estimator can then be used to reduce the variance of the estimation compared to a crude MC estimator, as confirmed with an idealized 1D problem of estimating the discretized intrinsic variance field of a diffusion-based covariance operator. However, projecting the variance of the MLMC estimator onto a spectral space revealed some discrepancy in the estimation of the different scales of the discretized field. In our experiments, the MLMC estimator was still able to still achieve a lower total variance by improving the estimation of the low-frequency (large-scale) components compared to the MC estimator, but at the expense of degrading the estimation in the higher-frequency (smaller-scale) components.

Inspired by multigrid methods, we proposed an improvement of the MLMC estimator by adding filtering operators, resulting in the F-MLMC estimator. Filtering out the high-frequency components of a discretized field before restriction and after prolongation removes spurious features, thus yielding a better estimation of both the small- and large-scale components. These improvements significantly impact the total variance of the F-MLMC estimators, which is also reduced compared to the MLMC estimators in our experiments. In the specific case of linear, symmetric, circulant simulators, we quantified the effects of grid transfer and filtering operators on the total variance of (F-)MLMC estimators, which allowed us to improve our understanding of the influence of each ingredient. The proposed F-MLMC estimators were applied to the problem of estimating the discretized intrinsic variance field of a 2D diffusion-based covariance operator with a non-uniform diffusivity field, which relies on non-linear simulators $\tilde{f}_\ell: \mathbf{X}_\ell \mapsto (\mathbf{A}_\ell \mathbf{X}_\ell) \odot (\mathbf{A}_\ell \mathbf{X}_\ell)$. The conclusions of these experiments were consistent with the theoretical results derived in the spectral analysis for linear, symmetric, circulant simulators. Specifically, F-MLMC estimators do reduce the variance in both the low and high frequencies compared to their unfiltered counterparts, thus improving the total variance. Even in experiments where MLMC estimators were not able to reduce (and, actually, did deteriorate) the variance compared to a crude MC estimator, F-MLMC estimators still achieved lower total variance.

It should be noted that, for the particular problem of estimating discretized variance fields considered in this paper, the proposed MLMC and F-MLMC estimators are not guaranteed to be almost surely non-negative. Although negative estimates were not encountered in our experiments, this is nonetheless a serious limitation of the multilevel estimators, as already pointed out for the MLMC estimation of the variance of random variables (possibly with values in Hilbert spaces) [2]. A similar issue exists for the estimation of covariance matrices, for which multilevel estimators are not guaranteed to be almost surely SPD [30], although advanced (but computationally expensive) approaches have been proposed to design multilevel estimators that are SPD by construction [38, 39]. These crucial issues still constitute an open research area.

Nonetheless, the investigations conducted in this paper and the proposed F-MLMC estimator expand the range of use of MLMC-like methods to discretized fields. In our study, the use of second-order Shapiro filters demonstrated the benefits of applying pre- and post-smoothing at each level of the MLMC estimators. A potential next step would be to investigate whether conditions can be derived for selecting the grid transfer and filtering operators, similar to the conditions stated in [12] for multigrid methods. Furthermore, extensions of the MLBLUE techniques [49, 50] to discretized fields may allow for the derivation of optimal spectral weights for each scale component of the discretized field to act as a post-prolongation filter [13, section 4.4], possibly in combination with the spectral pre-restriction smoothing technique of [31]. Finally, for the specific variance estimation problem described in section 2, sampling $\mathbf{A}\mathbf{x}$ requires solving (many) systems of linear equations of the form $\mathbf{M}\mathbf{u} = \mathbf{b}$, involving an SPD matrix $\mathbf{M} := \mathbf{W}(\mathbf{I} - \mathbf{\Delta})$. In our experiments, we solved these systems numerically using a Cholesky decomposition of \mathbf{M} . However, for large-scale problems, computing such a decomposition is not computationally tractable and sparse iterative methods are typically used instead [57]. An interesting research avenue would consist of exploiting further the hierarchical nature of MLMC techniques by combining them with multigrid iterative methods for solving the systems of linear equations, using the same grid hierarchy, along the lines of [32, 33].

A Choice of grid transfer operators

We detail here our choice of prolongation and restriction operators. Specifically, the prolongation operator $\mathbf{P} := \mathbf{P}_{\ell-1}^{\ell}$ between a coarse level $\ell - 1$ and the next fine level ℓ is designed such that it satisfies the norm-preserving property given by the first identity in eq. (17). By the definition of the weighted inner product eq. (6), this property can be recast as $\mathbf{x}_{\ell-1}^{\mathbf{T}} \mathbf{P}^{\mathbf{T}} \mathbf{W}_{\ell} \mathbf{P} \mathbf{x}_{\ell-1} = \mathbf{x}_{\ell-1}^{\mathbf{T}} \mathbf{W}_{\ell-1} \mathbf{x}_{\ell-1}$ for all $\mathbf{x}_{\ell} \in \mathbb{R}^{n_{\ell}}$, which, in turn, amounts to $\mathbf{P}^{\mathbf{T}} \mathbf{W}_{\ell} \mathbf{P} = \mathbf{W}_{\ell-1}$. For the particular choice $\mathbf{W}_{\ell} = n_{\ell}^{-1} \mathbf{I}_{n_{\ell}}$, for $\ell = 0, \dots, L$, this property becomes $\mathbf{P}^{\mathbf{T}} \mathbf{P} = (n_{\ell}/n_{\ell-1}) \mathbf{I}_{n_{\ell-1}}$. We note that the prolongation operator defined in eq. (16) satisfies this property with a refinement factor $n_{\ell}/n_{\ell-1} = 2$. Furthermore, for the variance estimation problem described in section 2 where normal random vectors need to be restricted to coarser grids, we want the second identity in eq. (17) to hold so that the restricted signals remain normally distributed with the same mean and variance on the coarser grids. With a linear restriction operator $\mathbf{R} := \mathbf{R}_{\ell}^{\ell-1}$, a zero-mean normal random vector trivially remains a zero-mean normal random vector when restricted to a coarser grid. Importantly, we require the restricted normal random vector to have a unit variance. To achieve this, we define $\mathbf{R} = \mathbf{V}_{\ell-1}^{-1} \mathbf{P}^{\mathbf{T}} \mathbf{V}_{\ell}$ as in eq. (16), which implies that

$$\mathbf{R}\mathbf{R}^{\mathbf{T}} = \mathbf{V}_{\ell-1}^{-1} \mathbf{P}^{\mathbf{T}} \mathbf{V}_{\ell} \mathbf{V}_{\ell}^{\mathbf{T}} \mathbf{P} (\mathbf{V}_{\ell-1}^{-1})^{\mathbf{T}} = \mathbf{V}_{\ell-1}^{-1} \mathbf{P}^{\mathbf{T}} \mathbf{W}_{\ell} \mathbf{P} (\mathbf{V}_{\ell-1}^{\mathbf{T}})^{-1} = \mathbf{V}_{\ell-1}^{-1} \mathbf{W}_{\ell-1} (\mathbf{V}_{\ell-1}^{\mathbf{T}})^{-1}, \quad (55)$$

where the last identity holds since $\mathbf{P}^{\mathbf{T}} \mathbf{W}_{\ell} \mathbf{P} = \mathbf{W}_{\ell-1}$. The decomposition $\mathbf{W}_{\ell-1} = \mathbf{V}_{\ell-1} \mathbf{V}_{\ell-1}^{\mathbf{T}}$ then implies that $\mathbf{R}\mathbf{R}^{\mathbf{T}} = \mathbf{I}_{n_{\ell-1}}$, and hence that the unit variance is conserved on the coarser grids.

B Orthogonality of the Hartley matrix

We focus here on a Hartley matrix \mathbf{H} of arbitrary size n ,

$$(\mathbf{H})_{j,k} := \frac{1}{\sqrt{n}} (\cos \alpha_{jk} + \sin \alpha_{jk}), \quad \alpha_{jk} := \frac{(2j+1)k\pi}{n}, \quad \forall j, k = 0, \dots, n-1. \quad (56)$$

We have, for $i, j = 0, \dots, n-1$,

$$(\mathbf{H}\mathbf{H}^\top)_{i,j} = \frac{1}{n} \sum_{k=0}^{n-1} (\cos \alpha_{ik} + \sin \alpha_{ik})(\cos \alpha_{jk} + \sin \alpha_{jk}) \quad (57)$$

$$= \frac{1}{n} \sum_{k=0}^{n-1} [\cos(\alpha_{ik} - \alpha_{jk}) + \sin(\alpha_{ik} + \alpha_{jk})] \quad (58)$$

$$= \frac{1}{n} \sum_{k=0}^{n-1} \cos \frac{2(i-j)k\pi}{n} + \frac{1}{n} \sum_{k=0}^{n-1} \sin \frac{2(i+j+1)k\pi}{n}. \quad (59)$$

From [21, 1.342 (1&2)], we deduce, for $i, j = 0, \dots, n-1$,

$$\sum_{k=0}^{n-1} \cos \frac{2(i-j)k\pi}{n} = n\delta_{ij}, \quad \sum_{k=0}^{n-1} \sin \frac{2(i+j+1)k\pi}{n} = 0, \quad (60)$$

where δ_{ij} denotes the Kronecker delta, thus proving that $\mathbf{H}\mathbf{H}^\top = \mathbf{I}_n$. Similarly,

$$(\mathbf{H}^\top\mathbf{H})_{i,j} = \frac{1}{n} \sum_{k=0}^{n-1} \cos \frac{(2k+1)(i-j)\pi}{n} + \frac{1}{n} \sum_{k=0}^{n-1} \sin \frac{(2k+1)(i+j)\pi}{n}, \quad (61)$$

and $\mathbf{H}^\top\mathbf{H} = \mathbf{I}_n$ follows from [21, 1.342 (3&4)].

C Reordering of the Hartley basis vectors

For the plots of the spectral variance, the columns of the 1D Hartley matrix \mathbf{H}_L used in eq. (20) are actually reordered so that they are sorted by increasing representable frequency on the corresponding discrete grid (see fig. 7, which depicts the Hartley basis vectors without reordering). Specifically, the new matrix with reordered columns is obtained as $\mathbf{H}_L\mathbf{\Pi}$, where $\mathbf{\Pi} = (\Pi_{j,k})_{j,k=0}^{n_L-1}$ is the permutation matrix defined by $\Pi_{j,2k} = \delta_{j,k}$ and $\Pi_{j,2k+1} = \delta_{j,n_L-k-1}$, for $j = 0, \dots, n_L-1$ and $k = 0, \dots, n_L/2-1$ (assuming n_L is even). The 2D Hartley matrix with reordered columns is constructed as the Kronecker product of two 1D Hartley matrices, each with reordered columns.

D Proof of eq. (27)

By linearity of the expectation operator, and denoting $\dot{\mathbf{X}}_L := \mathbf{X}_L - \mathbb{E}[\mathbf{X}_L]$, we have that $\mathcal{V}(Y_0) := \mathbb{E}[\|Y_0 - \mathbb{E}[Y_0]\|_{\mathbf{W}_L}^2] = \mathbb{E}[\|\mathbf{F}_0\dot{\mathbf{X}}_L\|_{\mathbf{W}_L}^2]$. Likewise, for $\ell = 1, \dots, L$, we have $\mathcal{V}(Y_\ell - Y_{\ell-1}) = \mathbb{E}[\|(\mathbf{F}_\ell - \mathbf{F}_{\ell-1})\dot{\mathbf{X}}_L\|_{\mathbf{W}_L}^2]$. Now, for any $\mathbf{M} \in \mathbb{R}^{n_L \times n_L}$,

$$\mathbb{E}[\|\mathbf{M}\dot{\mathbf{X}}_L\|_{\mathbf{W}_L}^2] = \mathbb{E}[(\mathbf{M}\dot{\mathbf{X}}_L)^\top \mathbf{W}_L (\mathbf{M}\dot{\mathbf{X}}_L)] = \text{tr} \mathbb{E}[\dot{\mathbf{X}}_L^\top \mathbf{M}^\top \mathbf{W}_L \mathbf{M} \dot{\mathbf{X}}_L] \quad (62)$$

$$= \mathbb{E}[\text{tr}(\dot{\mathbf{X}}_L^\top \mathbf{M}^\top \mathbf{W}_L \mathbf{M} \dot{\mathbf{X}}_L)] = \mathbb{E}[\text{tr}(\mathbf{M}^\top \mathbf{W}_L \mathbf{M} \dot{\mathbf{X}}_L \dot{\mathbf{X}}_L^\top)] \quad (63)$$

$$= \text{tr}(\mathbf{M}^\top \mathbf{W}_L \mathbf{M} \mathbb{E}[\dot{\mathbf{X}}_L \dot{\mathbf{X}}_L^\top]) = \text{tr}(\mathbf{M}^\top \mathbf{W}_L \mathbf{M} \mathbf{G}) \quad (64)$$

$$= \text{tr}((\mathbf{M}\mathbf{G}^{1/2})^\top \mathbf{W}_L (\mathbf{M}\mathbf{G}^{1/2})) = \|\mathbf{M}\mathbf{G}^{1/2}\|_{F, \mathbf{W}_L}^2, \quad (65)$$

where $\text{tr}(\cdot)$ denotes the matrix trace operator and \mathbf{G} denotes the covariance matrix of \mathbf{X}_L . Furthermore, assuming that $\mathbf{W}_L = w\mathbf{I}_{n_L}$ for some $w > 0$, for any $\mathbf{M} \in \mathbb{R}^{n_L \times n_L}$ and any orthogonal $\mathbf{Q} \in \mathbb{R}^{n_L \times n_L}$, we have $\|\mathbf{Q}^T \mathbf{M}\|_{F, \mathbf{W}_L}^2 = \text{tr}(w\mathbf{M}^T \mathbf{Q} \mathbf{Q}^T \mathbf{M}) = \text{tr}(\mathbf{M}^T \mathbf{W}_L \mathbf{M}) = \|\mathbf{M}\|_{F, \mathbf{W}_L}^2$, so that eq. (28) follows.

E Proof of eq. (29)

For $j, k = 0, \dots, n_0 - 1$,

$$(\mathbf{P}\mathbf{h}_k^0)_{2j} = (\mathbf{P}\mathbf{h}_k^0)_{2j+1} = (\mathbf{h}_k^0)_j = \frac{\sqrt{2}}{\sqrt{n_1}} \left[\cos \frac{(4j+2)k\pi}{n_1} + \sin \frac{(4j+2)k\pi}{n_1} \right]. \quad (66)$$

Upon writing $(4j+2)k\pi = (4j+1)k\pi + k\pi$ and applying elementary trigonometric identities,

$$(\mathbf{P}\mathbf{h}_k^0)_{2j} = \sqrt{2}c_k(\mathbf{h}_k^1)_{2j} + \frac{\sqrt{2}}{\sqrt{n_1}} \left[\sin \frac{k\pi}{n_1} \left(\cos \frac{(4j+1)k\pi}{n_1} - \sin \frac{(4j+1)k\pi}{n_1} \right) \right]. \quad (67)$$

Noticing that

$$\sin \frac{k\pi}{n_1} = \sin \left(\frac{(n_0+k)\pi}{2n_0} - \frac{\pi}{2} \right) = -c_{n_0+k}, \quad (68)$$

$$\cos \frac{(4j+1)k\pi}{n_1} = \cos \left(\frac{(4j+1)(n_0+k)\pi}{n_1} - \frac{\pi}{2} \right) = \sin \frac{(4j+1)k\pi}{n_1}, \quad (69)$$

$$\sin \frac{(4j+1)k\pi}{n_1} = \sin \left(\frac{(4j+1)(n_0+k)\pi}{n_1} - \frac{\pi}{2} \right) = -\cos \frac{(4j+1)k\pi}{n_1}, \quad (70)$$

we conclude that $(\mathbf{P}\mathbf{h}_k^0)_{2j} = \sqrt{2}(c_k(\mathbf{h}_k^1)_{2j} - c_{n_0+k}(\mathbf{h}_{n_0+k}^1)_{2j})$. A similar derivation allows us to show that $(\mathbf{P}\mathbf{h}_k^0)_{2j+1} = \sqrt{2}(c_k(\mathbf{h}_k^1)_{2j+1} - c_{n_0+k}(\mathbf{h}_{n_0+k}^1)_{2j+1})$, thus proving eq. (29).

F Proof of eq. (31)

For $j = 0, \dots, n_0 - 1$ and $k = 0, \dots, 2n_0 - 1$,

$$(\mathbf{R}\mathbf{h}_k^1)_j = \frac{1}{\sqrt{2}}((\mathbf{h}_k^1)_{2j} + (\mathbf{h}_k^1)_{2j+1}) \quad (71)$$

$$= \frac{1}{\sqrt{2n_1}} \left[\cos \frac{(4j+1)k\pi}{n_1} + \cos \frac{(4j+3)k\pi}{n_1} + \sin \frac{(4j+1)k\pi}{n_1} + \sin \frac{(4j+3)k\pi}{n_1} \right] \quad (72)$$

$$= \frac{1}{\sqrt{2n_1}} \left[2 \cos \frac{(8j+4)k\pi}{2n_1} \cos \frac{2k\pi}{2n_1} + 2 \sin \frac{(8j+4)k\pi}{2n_1} \cos \frac{2k\pi}{2n_1} \right] \quad (73)$$

$$= \frac{c_k}{\sqrt{n_0}} \left[\cos \frac{(2j+1)k\pi}{n_0} + \sin \frac{(2j+1)k\pi}{n_0} \right]. \quad (74)$$

Hence, for $j, k = 0, \dots, n_0 - 1$, it follows immediately that $\mathbf{R}\mathbf{h}_k^1 = c_k \mathbf{h}_k^0$. Furthermore,

$$(\mathbf{R}\mathbf{h}_{n_0+k}^1)_j = \frac{c_{n_0+k}}{\sqrt{n_0}} \left[\cos \left(\frac{(2j+1)k\pi}{n_0} + \pi \right) + \sin \left(\frac{(2j+1)k\pi}{n_0} + \pi \right) \right] = -c_{n_0+k} \mathbf{h}_k^0, \quad (75)$$

thus proving eq. (31).

G Symmetric circulant matrices are diagonalizable in the Hartley basis

In this appendix, we prove theorem 2 below, which states that symmetric, circulant matrices can be diagonalized in the cell-centered Hartley basis \mathbf{H} defined by eq. (56). To do so, we start by recalling or proving results on the node-centered Fourier basis $\check{\mathbf{F}} \in \mathbb{C}^{n \times n}$ and Hartley bases $\check{\mathbf{H}}^\pm \in \mathbb{R}^{n \times n}$ defined by

$$\check{\mathbf{F}} := \check{\mathbf{H}}_c + i\check{\mathbf{H}}_s, \quad \check{\mathbf{H}}^\pm := \check{\mathbf{H}}_c \pm \check{\mathbf{H}}_s, \quad (\check{\mathbf{H}}_c)_{j,k} := \frac{1}{\sqrt{n}} \cos \frac{2jk\pi}{n}, \quad (\check{\mathbf{H}}_s)_{j,k} := \frac{1}{\sqrt{n}} \sin \frac{2jk\pi}{n}, \quad (76)$$

where $i \in \mathbb{C}$ denotes the unit imaginary number such that $i^2 = -1$. It is clear that $\check{\mathbf{H}}_c$ and $\check{\mathbf{H}}_s$ are real, symmetric matrices, and hence so are $\check{\mathbf{H}}^\pm$, while $\check{\mathbf{F}}$ is a complex, symmetric (but not Hermitian) matrix. Furthermore, $\check{\mathbf{F}}$ is unitary (see, e.g., [11]), i.e., $\check{\mathbf{F}}^* \check{\mathbf{F}} = \check{\mathbf{F}} \check{\mathbf{F}}^* = \mathbf{I}_n$, where $\check{\mathbf{F}}^* = \check{\mathbf{H}}_c - i\check{\mathbf{H}}_s$ is the Hermitian transpose of $\check{\mathbf{F}}$.

Lemma 1. $\check{\mathbf{H}}_c$ and $\check{\mathbf{H}}_s$ are such that

$$\check{\mathbf{H}}_c^2 + \check{\mathbf{H}}_s^2 = \mathbf{I}_n, \quad \check{\mathbf{H}}_c \check{\mathbf{H}}_s = \check{\mathbf{H}}_s \check{\mathbf{H}}_c = \mathbf{0}_n, \quad \check{\mathbf{H}}_c \mathbf{1}_n = \sqrt{n} \mathbf{e}_1, \quad \check{\mathbf{H}}_s \mathbf{1}_n = \mathbf{0}_n, \quad (77)$$

where $\mathbf{0}_n := (0, \dots, 0)^T \in \mathbb{R}^n$, $\mathbf{1}_n := (1, \dots, 1)^T \in \mathbb{R}^n$, and \mathbf{e}_1 denotes the first column of \mathbf{I}_n .

Proof. The first two identities follow from [4, Lemma 1], while the last two identities follow from [21, 1.342 (1&2)]. \square

Corollary 1. $\check{\mathbf{H}}^\pm \mathbf{1}_n = \sqrt{n} \mathbf{e}_1$.

Corollary 2. $\check{\mathbf{H}}^\pm$ are orthogonal, i.e., $(\check{\mathbf{H}}^\pm)^2 = \mathbf{I}_n$. Furthermore, $\check{\mathbf{H}}^+ \check{\mathbf{H}}^- = \check{\mathbf{H}}^- \check{\mathbf{H}}^+ = \check{\mathbf{F}}^2$.

Proof. By the definitions eq. (76) and lemma 1, we have

$$\check{\mathbf{H}}^\pm \mathbf{1}_n = \check{\mathbf{H}}_c \mathbf{1}_n \pm \check{\mathbf{H}}_s \mathbf{1}_n = \check{\mathbf{H}}_c \mathbf{1}_n = \sqrt{n} \mathbf{e}_1, \quad (78)$$

$$(\check{\mathbf{H}}^\pm)^2 = (\check{\mathbf{H}}_c^2 + \check{\mathbf{H}}_s^2) \pm (\check{\mathbf{H}}_c \check{\mathbf{H}}_s + \check{\mathbf{H}}_s \check{\mathbf{H}}_c) = \check{\mathbf{H}}_c^2 + \check{\mathbf{H}}_s^2 = \mathbf{I}_n, \quad (79)$$

$$\check{\mathbf{F}}^2 = \check{\mathbf{H}}_c^2 - \check{\mathbf{H}}_s^2 + i(\check{\mathbf{H}}_c \check{\mathbf{H}}_s + \check{\mathbf{H}}_s \check{\mathbf{H}}_c) = \check{\mathbf{H}}_c^2 - \check{\mathbf{H}}_s^2, \quad (80)$$

$$\check{\mathbf{H}}^- \check{\mathbf{H}}^+ = \check{\mathbf{H}}_c^2 - \check{\mathbf{H}}_s^2 + (\check{\mathbf{H}}_c \check{\mathbf{H}}_s - \check{\mathbf{H}}_s \check{\mathbf{H}}_c) = \check{\mathbf{F}}^2 = \check{\mathbf{H}}^+ \check{\mathbf{H}}^-. \quad (81)$$

\square

Lemma 2. Let $\mathbf{A} = \text{Circ}(\mathbf{a}) \in \mathbb{R}^{n \times n}$ be a symmetric, circulant matrix whose first column is $\mathbf{a} = (a_k)_{k=0}^{n-1} \in \mathbb{R}^n$, with $a_{n-i} = a_i$, for $i = 1, \dots, n-1$. Then $\check{\mathbf{H}}_c \mathbf{A} \check{\mathbf{H}}_s + \check{\mathbf{H}}_s \mathbf{A} \check{\mathbf{H}}_c = \check{\mathbf{H}}_c \mathbf{A} \check{\mathbf{H}}_s - \check{\mathbf{H}}_s \mathbf{A} \check{\mathbf{H}}_c = \mathbf{0}_n$.

Proof. Proven in the intermediary steps of the proof of [4, Theorem 1]. \square

Theorem 1. Let $\mathbf{A} = \text{Circ}(\mathbf{a}) \in \mathbb{R}^{n \times n}$ be a symmetric, circulant matrix whose first column is $\mathbf{a} = (a_k)_{k=0}^{n-1} \in \mathbb{R}^n$, with $a_{n-i} = a_i$, for $i = 1, \dots, n-1$. Then $\check{\mathbf{H}}^+ \mathbf{A} \check{\mathbf{H}}^+ = \check{\mathbf{H}}^- \mathbf{A} \check{\mathbf{H}}^- = \mathbf{\Lambda}$, where $\mathbf{\Lambda} = \sqrt{n} \text{Diag}(\check{\mathbf{H}}^+ \mathbf{a}) = \sqrt{n} \text{Diag}(\check{\mathbf{H}}^- \mathbf{a}) = \sqrt{n} \text{Diag}(\check{\mathbf{H}}_c \mathbf{a})$.

Proof. The fact that $\check{\mathbf{H}}^+ \mathbf{A} \check{\mathbf{H}}^+ = \sqrt{n} \text{Diag}(\check{\mathbf{H}}^+ \mathbf{a}) = \mathbf{\Lambda} = \check{\mathbf{H}}_c \mathbf{A} \check{\mathbf{H}}_c + \check{\mathbf{H}}_s \mathbf{A} \check{\mathbf{H}}_s$ follows from [4, Theorem 1], since symmetric, circulant matrices belong to the larger class of matrices considered in [4]. Then, from the definition of $\check{\mathbf{H}}^-$ and lemma 2, we have

$$\check{\mathbf{H}}^- \mathbf{A} \check{\mathbf{H}}^- = (\check{\mathbf{H}}_c \mathbf{A} \check{\mathbf{H}}_c + \check{\mathbf{H}}_s \mathbf{A} \check{\mathbf{H}}_s) - (\check{\mathbf{H}}_c \mathbf{A} \check{\mathbf{H}}_s + \check{\mathbf{H}}_s \mathbf{A} \check{\mathbf{H}}_c) = \check{\mathbf{H}}_c \mathbf{A} \check{\mathbf{H}}_c + \check{\mathbf{H}}_s \mathbf{A} \check{\mathbf{H}}_s = \mathbf{\Lambda}. \quad (82)$$

Finally, from lemma 1 and corollary 1,

$$\text{diag}(\mathbf{\Lambda}) = \mathbf{\Lambda}\mathbf{1}_n = \check{\mathbf{H}}^- \mathbf{A} \check{\mathbf{H}}^- \mathbf{1}_n = \check{\mathbf{H}}_c \mathbf{A} \check{\mathbf{H}}_c \mathbf{1}_n + \check{\mathbf{H}}_s \mathbf{A} \check{\mathbf{H}}_s \mathbf{1}_n = \sqrt{n} \check{\mathbf{H}}^- \mathbf{A} \mathbf{e}_1 = \sqrt{n} \check{\mathbf{H}}_c \mathbf{A} \mathbf{e}_1, \quad (83)$$

which concludes the proof, since $\mathbf{A} \mathbf{e}_1 = \mathbf{a}$. \square

Corollary 3. Let $\mathbf{A} = \text{Circ}(\mathbf{a}) \in \mathbb{R}^{n \times n}$ be a symmetric, circulant matrix and let $\mathbf{\Lambda}$ be defined as in theorem 1. Then $\check{\mathbf{H}}^+ \mathbf{A} \check{\mathbf{H}}^- = \check{\mathbf{H}}^- \mathbf{A} \check{\mathbf{H}}^+ = \mathbf{\Lambda} \check{\mathbf{F}}^2 = \check{\mathbf{F}}^2 \mathbf{\Lambda}$.

Proof. From theorem 1 and corollary 2, we have

$$\check{\mathbf{H}}^+ \mathbf{A} \check{\mathbf{H}}^- = \check{\mathbf{H}}^+ \mathbf{A} \check{\mathbf{H}}^+ \check{\mathbf{H}}^+ \check{\mathbf{H}}^- = \check{\mathbf{H}}^+ \mathbf{A} \check{\mathbf{H}}^+ \check{\mathbf{F}}^2 = \mathbf{\Lambda} \check{\mathbf{F}}^2, \quad (84)$$

$$\check{\mathbf{H}}^- \mathbf{A} \check{\mathbf{H}}^+ = \check{\mathbf{H}}^- \mathbf{A} \check{\mathbf{H}}^- \check{\mathbf{H}}^- \check{\mathbf{H}}^+ = \check{\mathbf{H}}^- \mathbf{A} \check{\mathbf{H}}^- \check{\mathbf{F}}^2 = \mathbf{\Lambda} \check{\mathbf{F}}^2, \quad (85)$$

$$(\check{\mathbf{H}}^+ \mathbf{A} \check{\mathbf{H}}^-)^\top = (\mathbf{\Lambda} \check{\mathbf{F}}^2)^\top = \check{\mathbf{F}}^2 \mathbf{\Lambda} = \check{\mathbf{H}}^- \mathbf{A} \check{\mathbf{H}}^+ = \mathbf{\Lambda} \check{\mathbf{F}}^2, \quad (86)$$

where the last row follows from the symmetry of \mathbf{A} , $\check{\mathbf{H}}^\pm$ and $\check{\mathbf{F}}^2$. \square

Lemma 3. $\mathbf{H} = \check{\mathbf{H}}^+ \mathbf{C} + \check{\mathbf{H}}^- \mathbf{S}$, with $\mathbf{C} := \text{Diag}(\{\cos \frac{k\pi}{n}\}_{k=0}^{n-1})$ and $\mathbf{S} := \text{Diag}(\{\sin \frac{k\pi}{n}\}_{k=0}^{n-1})$.

Proof. From elementary trigonometric identities, we have

$$\cos \frac{(2j+1)k\pi}{n} = \cos \frac{2jk\pi}{n} \cos \frac{k\pi}{n} - \sin \frac{2jk\pi}{n} \sin \frac{k\pi}{n}, \quad (87)$$

$$\sin \frac{(2j+1)k\pi}{n} = \sin \frac{2jk\pi}{n} \cos \frac{k\pi}{n} - \cos \frac{2jk\pi}{n} \sin \frac{k\pi}{n}, \quad (88)$$

then lemma 3 follows. \square

Lemma 4. $\mathbf{C} \check{\mathbf{F}}^2 \mathbf{S} + \mathbf{S} \check{\mathbf{F}}^2 \mathbf{C} = \mathbf{0}_n$, where \mathbf{C} and \mathbf{S} are defined as in lemma 3.

Proof. From [4, Lemma 1], we have that, for $j, k = 0, \dots, n-1$, $(\check{\mathbf{F}}^2)_{j,k} = 1$ if $j = k = 0$ or $j+k = n$, and $(\check{\mathbf{F}}^2)_{j,k} = 0$ otherwise. Moreover, $(\mathbf{C} \check{\mathbf{F}}^2 \mathbf{S})_{j,k} = (\check{\mathbf{F}}^2)_{j,k} \cos \frac{j\pi}{n} \sin \frac{k\pi}{n}$, and, by symmetry, $\mathbf{S} \check{\mathbf{F}}^2 \mathbf{C} = (\mathbf{C} \check{\mathbf{F}}^2 \mathbf{S})^\top$. Now, if $j = k = 0$, $(\mathbf{C} \check{\mathbf{F}}^2 \mathbf{S})_{j,k} = (\mathbf{S} \check{\mathbf{F}}^2 \mathbf{C})_{j,k} = 0$ trivially. Otherwise, if $j \neq 0$, $k \neq 0$, and $j+k \neq n$, $(\mathbf{C} \check{\mathbf{F}}^2 \mathbf{S})_{j,k} = (\mathbf{S} \check{\mathbf{F}}^2 \mathbf{C})_{j,k} = 0$. Finally, if $j+k = n$, elementary trigonometric identities induce

$$(\mathbf{C} \check{\mathbf{F}}^2 \mathbf{S})_{j,k} = \cos \frac{j\pi}{n} \sin \frac{(n-j)\pi}{n} = \cos \frac{j\pi}{n} \sin \left(\pi - \frac{j\pi}{n} \right) = \cos \frac{j\pi}{n} \sin \frac{j\pi}{n}, \quad (89)$$

$$(\mathbf{C} \check{\mathbf{F}}^2 \mathbf{S})_{k,j} = \sin \frac{j\pi}{n} \cos \frac{(n-j)\pi}{n} = \sin \frac{j\pi}{n} \cos \left(\pi - \frac{j\pi}{n} \right) = -\cos \frac{j\pi}{n} \sin \frac{j\pi}{n}, \quad (90)$$

so that $(\mathbf{C} \check{\mathbf{F}}^2 \mathbf{S} + \mathbf{S} \check{\mathbf{F}}^2 \mathbf{C})_{j,k} = (\mathbf{C} \check{\mathbf{F}}^2 \mathbf{S})_{j,k} + (\mathbf{C} \check{\mathbf{F}}^2 \mathbf{S})_{k,j} = 0$, thus completing the proof. \square

We are now ready to state and prove theorem 2.

Theorem 2. Let $\mathbf{A} = \text{Circ}(\mathbf{a}) \in \mathbb{R}^{n \times n}$ be a symmetric, circulant matrix and let $\mathbf{\Lambda}$ be defined as in theorem 1. Then $\mathbf{H}^\top \mathbf{A} \mathbf{H} = \mathbf{\Lambda}$.

Proof. Starting from the expression of lemma 3, and applying theorem 1, corollary 3 and lemma 4, we obtain

$$\mathbf{H}^\top \mathbf{A} \mathbf{H} = \mathbf{C} \check{\mathbf{H}}^+ \mathbf{A} \check{\mathbf{H}}^+ \mathbf{C} + \mathbf{S} \check{\mathbf{H}}^- \mathbf{A} \check{\mathbf{H}}^- \mathbf{S} + \mathbf{C} \check{\mathbf{H}}^+ \mathbf{A} \check{\mathbf{H}}^- \mathbf{S} + \mathbf{S} \check{\mathbf{H}}^- \mathbf{A} \check{\mathbf{H}}^+ \mathbf{C} \quad (91)$$

$$= \mathbf{C} \mathbf{\Lambda} \mathbf{C} + \mathbf{S} \mathbf{\Lambda} \mathbf{S} + \mathbf{C} \mathbf{\Lambda} \check{\mathbf{F}}^2 \mathbf{S} + \mathbf{S} \mathbf{\Lambda} \check{\mathbf{F}}^2 \mathbf{C} = \mathbf{\Lambda} (\mathbf{C}^2 + \mathbf{S}^2 + \mathbf{C} \check{\mathbf{F}}^2 \mathbf{S} + \mathbf{S} \check{\mathbf{F}}^2 \mathbf{C}), \quad (92)$$

so that $\mathbf{H}^\top \mathbf{A} \mathbf{H} = \mathbf{\Lambda} (\mathbf{C}^2 + \mathbf{S}^2) = \mathbf{\Lambda}$ since $\mathbf{C}^2 + \mathbf{S}^2 = \mathbf{I}_n$ by elementary trigonometry. \square

H Proof of the optimality of the Galerkin operator

Let $n_1, n_0 \in \mathbb{N}$ be such that $n_1 > n_0 > 0$, and let $\mathbf{A}_1 \in \mathbb{R}^{n_1 \times n_1}$ and $\mathbf{A}_0 \in \mathbb{R}^{n_0 \times n_0}$ be two linear operators. Let $\mathbf{R} \in \mathbb{R}^{n_0 \times n_1}$ and $\mathbf{P} \in \mathbb{R}^{n_1 \times n_0}$ be a restriction operator and a prolongation operator, respectively, such that $\mathbf{R}\mathbf{R}^\top = \mathbf{I}_{n_0}$ and $\mathbf{P} = \alpha\mathbf{R}^\top$, for some $\alpha \in \mathbb{R}$. We seek the operator \mathbf{A}_0^* that minimizes $\|\mathbf{A}_1 - \mathbf{P}\mathbf{A}_0\mathbf{R}\|_{\mathbb{F}, \mathbf{W}_1}^2$ among the linear operators $\mathbf{A}_0 \in \mathbb{R}^{n_0 \times n_0}$. We restrict ourselves to the case where $\mathbf{W}_1 = w\mathbf{I}_{n_1}$, with $w > 0$, so that

$$\mathbf{A}_0^* := \arg \min_{\mathbf{A}_0 \in \mathbb{R}^{n_0 \times n_0}} \|\mathbf{A}_1 - \mathbf{P}\mathbf{A}_0\mathbf{R}\|_{\mathbb{F}, \mathbf{W}_1}^2 = \arg \min_{\mathbf{A}_0 \in \mathbb{R}^{n_0 \times n_0}} \|\mathbf{A}_1 - \mathbf{P}\mathbf{A}_0\mathbf{R}\|_{\mathbb{F}}^2, \quad (93)$$

where $\|\cdot\|_{\mathbb{F}}$ denotes the classical (unweighted) Frobenius norm. We start by writing

$$\|\mathbf{A}_1 - \mathbf{P}\mathbf{A}_0\mathbf{R}\|_{\mathbb{F}}^2 = \|\mathbf{A}_1 - \mathbf{P}\mathbf{A}_0\mathbf{R}\|_{\mathbb{F}}^2 = \|\text{vec}(\mathbf{A}_1 - \mathbf{P}\mathbf{A}_0\mathbf{R})\|_{\mathbb{F}}^2 \quad (94)$$

$$= \|\text{vec}(\mathbf{A}_1) - \text{vec}(\mathbf{P}\mathbf{A}_0\mathbf{R})\|_2^2 = \|\text{vec}(\mathbf{A}_1) - (\mathbf{R}^\top \otimes \mathbf{P}) \text{vec}(\mathbf{A}_1)\|_2^2, \quad (95)$$

so that eq. (93) is recast as an ordinary linear least squares problem whose solution is

$$\text{vec}(\mathbf{A}_0^*) = ((\mathbf{R}^\top \otimes \mathbf{P})^\top (\mathbf{R}^\top \otimes \mathbf{P}))^{-1} (\mathbf{R}^\top \otimes \mathbf{P})^\top \text{vec}(\mathbf{A}_1) \quad (96)$$

$$= ((\mathbf{R} \otimes \mathbf{P}^\top)(\mathbf{R}^\top \otimes \mathbf{P}))^{-1} (\mathbf{R} \otimes \mathbf{P}^\top) \text{vec}(\mathbf{A}_1) \quad (97)$$

$$= (\mathbf{R}\mathbf{R}^\top \otimes \mathbf{P}^\top\mathbf{P})^{-1} \text{vec}(\mathbf{P}^\top\mathbf{A}_1\mathbf{R}^\top) = (\mathbf{I}_{n_0} \otimes \alpha^2\mathbf{I}_{n_0})^{-1} \text{vec}((\alpha\mathbf{R})\mathbf{A}_1(\alpha^{-1}\mathbf{P})) \quad (98)$$

$$= \alpha^{-2}(\mathbf{I}_{n_0} \otimes \mathbf{I}_{n_0}) \text{vec}(\mathbf{R}\mathbf{A}_1\mathbf{P}) = \alpha^{-2} \text{vec}(\mathbf{R}\mathbf{A}_1\mathbf{P}), \quad (99)$$

thus proving that $\mathbf{A}_0^* = \alpha^{-2}\mathbf{R}\mathbf{A}_1\mathbf{P}$.

I Proof of eqs. (43) and (44)

We start by looking at the effect of the Shapiro filter on the fine Hartley basis vectors, $(\mathbf{S}_1\mathbf{h}_k^1)_j = \frac{1}{4} [(\mathbf{h}_k^1)_{j-1} + 2(\mathbf{h}_k^1)_j + (\mathbf{h}_k^1)_{j+1}]$. Elementary trigonometric identities imply that, for $j, k = 0, \dots, n_1 - 1$,

$$\cos \frac{(2j-1)k\pi}{n_1} + \cos \frac{(2j+1)k\pi}{n_1} = 2c_k \cos \frac{2jk\pi}{n_1}, \quad (100)$$

$$\cos \frac{(2j+1)k\pi}{n_1} + \cos \frac{(2j+3)k\pi}{n_1} = 2c_k \cos \frac{(2j+2)k\pi}{n_1}, \quad (101)$$

$$\sin \frac{(2j-1)k\pi}{n_1} + \sin \frac{(2j+1)k\pi}{n_1} = 2c_k \sin \frac{2jk\pi}{n_1}, \quad (102)$$

$$\sin \frac{(2j+1)k\pi}{n_1} + \sin \frac{(2j+3)k\pi}{n_1} = 2c_k \sin \frac{(2j+2)k\pi}{n_1}, \quad (103)$$

leading to

$$(\mathbf{S}_1\mathbf{h}_k^1)_j = \frac{c_k}{2} \left[\cos \frac{2jk\pi}{n_1} + \cos \frac{(2j+2)k\pi}{n_1} + \sin \frac{2jk\pi}{n_1} + \sin \frac{(2j+2)k\pi}{n_1} \right] = c_k^2 (\mathbf{h}_k^1)_j, \quad (104)$$

where the last identity is obtained by applying the same trigonometric identities as for eqs. (100) to (103), and thus showing that $\mathbf{S}_1\mathbf{h}_k^1 = c_k^2\mathbf{h}_k^1$, for $k = 0, \dots, n_1 - 1$. Then, eq. (29) implies that, for $k = 0, \dots, n_0 - 1$, $\mathbf{P}\mathbf{h}_k^0 = \mathbf{S}_1\mathbf{P}\mathbf{h}_k^0 = \sqrt{2} [c_k\mathbf{S}_1\mathbf{h}_k^1 - c_{n_0+k}\mathbf{S}_1\mathbf{h}_{n_0+k}^1]$, from which eq. (43) follows. Furthermore, eq. (44) follows immediately from the direct application of eq. (31) to $\bar{\mathbf{R}}\mathbf{h}_k^0 = \mathbf{R}\mathbf{S}_1\mathbf{h}_k^0 = c_k^2\mathbf{R}\mathbf{h}_k^0$.

Acknowledgments

This project has received financial support from the CNRS (Centre National de la Recherche Scientifique) through the 80|Prime program and the French national program LEFE (Les Enveloppes Fluides et l'Environnement).

For the purpose of Open Access, a CC-BY public copyright licence has been applied by the authors to the present document and will be applied to all subsequent versions up to the Author Accepted Manuscript arising from this submission.

References

- [1] C. Bekas, E. Kokiopoulou, and Y. Saad. “An Estimator for the Diagonal of a Matrix.” In: *Applied Numerical Mathematics* 57.11-12 (2007), pp. 1214–1229. ISSN: 01689274. DOI: [10.1016/j.apnum.2007.01.003](https://doi.org/10.1016/j.apnum.2007.01.003).
- [2] C. Bierig and A. Chernov. “Convergence analysis of multilevel Monte Carlo variance estimators and application for random obstacle problems.” In: *Numerische Mathematik* 130.4 (2015), pp. 579–613. ISSN: 0945-3245. DOI: [10.1007/s00211-014-0676-3](https://doi.org/10.1007/s00211-014-0676-3).
- [3] C. Bierig and A. Chernov. “Estimation of arbitrary order central statistical moments by the multilevel Monte Carlo method.” In: *Stochastics and Partial Differential Equations Analysis and Computations* 4.1 (2016), pp. 3–40. ISSN: 2194-041X. DOI: [10.1007/s40072-015-0063-9](https://doi.org/10.1007/s40072-015-0063-9).
- [4] D. Bini and P. Favati. “On a Matrix Algebra Related to the Discrete Hartley Transform.” In: *SIAM Journal on Matrix Analysis and Applications* 14.2 (1993), pp. 500–507. ISSN: 0895-4798. DOI: [10.1137/0614035](https://doi.org/10.1137/0614035).
- [5] R. N. Bracewell. “Discrete Hartley Transform.” In: *JOSA* 73.12 (1983), pp. 1832–1835. DOI: [10.1364/JOSA.73.001832](https://doi.org/10.1364/JOSA.73.001832).
- [6] A. Brandt. “Guide to Multigrid Development.” In: *Multigrid Methods*. Ed. by W. Hackbusch and U. Trottenberg. Lecture Notes in Mathematics. Berlin, Heidelberg: Springer, 1982, pp. 220–312. ISBN: 978-3-540-39544-7. DOI: [10.1007/BFb0069930](https://doi.org/10.1007/BFb0069930).
- [7] W. L. Briggs, V. E. Henson, and S. F. McCormick. *A Multigrid Tutorial, Second Edition*. Second. Society for Industrial and Applied Mathematics, 2000. ISBN: 978-0-89871-462-3. DOI: [10.1137/1.9780898719505](https://doi.org/10.1137/1.9780898719505).
- [8] T. Bui-Thanh, O. Ghattas, J. Martin, and G. Stadler. “A Computational Framework for Infinite-Dimensional Bayesian Inverse Problems Part I: The Linearized Case, with Application to Global Seismic Inversion.” In: *SIAM Journal on Scientific Computing* 35.6 (2013), A2494–A2523. ISSN: 1064-8275, 1095-7197. DOI: [10.1137/12089586X](https://doi.org/10.1137/12089586X).
- [9] K. A. Cliffe, M. B. Giles, R. Scheichl, and A. L. Teckentrup. “Multilevel Monte Carlo Methods and Applications to Elliptic PDEs with Random Coefficients.” In: *Computing and Visualization in Science* 14.1 (2011), pp. 3–15. ISSN: 1432-9360, 1433-0369. DOI: [10.1007/s00791-011-0160-x](https://doi.org/10.1007/s00791-011-0160-x).
- [10] M. Croci, K. E. Willcox, and S. J. Wright. “Multi-Output Multilevel Best Linear Unbiased Estimators via Semidefinite Programming.” In: *Computer Methods in Applied Mechanics and Engineering* 413 (2023), p. 116130. ISSN: 00457825. DOI: [10.1016/j.cma.2023.116130](https://doi.org/10.1016/j.cma.2023.116130).
- [11] P. J. Davis. *Circulant Matrices: Second Edition*. 2nd. American Mathematical Society, 2012. ISBN: 978-0-8218-9165-0. URL: <https://bookstore.ams.org/chel-338>.

- [12] L. Debreu, E. Neveu, E. Simon, F.-X. Le Dimet, and A. Vidard. “Multigrid solvers and multigrid preconditioners for the solution of variational data assimilation problems.” In: *Quarterly Journal of the Royal Meteorological Society* 142.694 (2016), pp. 515–528. ISSN: 1477-870X. DOI: [10.1002/qj.2676](https://doi.org/10.1002/qj.2676).
- [13] M. Destouches, P. Mycek, and S. Gürol. *Multivariate Extensions of the Multilevel Best Linear Unbiased Estimator for Ensemble-Variational Data Assimilation*. 2023. DOI: [10.48550/arXiv.2306.07017](https://doi.org/10.48550/arXiv.2306.07017).
- [14] T. O. Dixon, J. E. Warner, G. F. Bomarito, and A. A. Gorodetsky. *Covariance Expressions for Multi-Fidelity Sampling with Multi-Output, Multi-Statistic Estimators: Application to Approximate Control Variates*. 2023. DOI: [10.48550/arXiv.2310.00125](https://doi.org/10.48550/arXiv.2310.00125).
- [15] D. Drzisga, B. Gmeiner, U. Råde, R. Scheichl, and B. Wohlmuth. “Scheduling Massively Parallel Multigrid for Multilevel Monte Carlo Methods.” In: *SIAM Journal on Scientific Computing* 39.5 (2017), S873–S897. ISSN: 1064-8275. DOI: [10.1137/16M1083591](https://doi.org/10.1137/16M1083591).
- [16] F. Falissard. “Genuinely multi-dimensional explicit and implicit generalized Shapiro filters for weather forecasting, computational fluid dynamics and aeroacoustics.” In: *Journal of Computational Physics* 253 (2013), pp. 344–367. ISSN: 0021-9991. DOI: [10.1016/j.jcp.2013.07.001](https://doi.org/10.1016/j.jcp.2013.07.001).
- [17] F. Falissard. “Uneven-order decentered Shapiro filters for boundary filtering.” In: *Journal of Computational Physics* 292 (2015), pp. 168–175. ISSN: 0021-9991. DOI: [10.1016/j.jcp.2015.03.003](https://doi.org/10.1016/j.jcp.2015.03.003).
- [18] M. B. Giles. “Multilevel Monte Carlo methods.” In: *Acta Numerica* 24 (2015), pp. 259–328. ISSN: 0962-4929, 1474-0508. DOI: [10.1017/S096249291500001X](https://doi.org/10.1017/S096249291500001X).
- [19] M. B. Giles. “Multilevel Monte Carlo Path Simulation.” In: *Operations Research* 56.3 (2008), pp. 607–617. ISSN: 0030-364X. DOI: [10.1287/opre.1070.0496](https://doi.org/10.1287/opre.1070.0496).
- [20] A. A. Gorodetsky, G. Geraci, M. S. Eldred, and J. D. Jakeman. “A Generalized Approximate Control Variate Framework for Multifidelity Uncertainty Quantification.” In: *Journal of Computational Physics* 408 (2020), p. 109257. ISSN: 0021-9991. DOI: [10.1016/j.jcp.2020.109257](https://doi.org/10.1016/j.jcp.2020.109257).
- [21] I. S. Gradshteyn and I. M. Ryshik. *Table of Integrals, Series, and Products*. 8th. Elsevier, 2015. ISBN: 978-0-12-384933-5. URL: <https://linkinghub.elsevier.com/retrieve/pii/C20100648395>.
- [22] I. G. Graham, F. Y. Kuo, D. Nuyens, R. Scheichl, and I. H. Sloan. “Analysis of Circulant Embedding Methods for Sampling Stationary Random Fields.” In: *SIAM Journal on Numerical Analysis* 56.3 (2018), pp. 1871–1895. ISSN: 0036-1429, 1095-7170. DOI: [10.1137/17M1149730](https://doi.org/10.1137/17M1149730).
- [23] I. Graham, F. Kuo, D. Nuyens, R. Scheichl, and I. Sloan. “Quasi-Monte Carlo Methods for Elliptic PDEs with Random Coefficients and Applications.” In: *Journal of Computational Physics* 230.10 (2011), pp. 3668–3694. ISSN: 00219991. DOI: [10.1016/j.jcp.2011.01.023](https://doi.org/10.1016/j.jcp.2011.01.023).
- [24] A. Gregory, C. J. Cotter, and S. Reich. “Multilevel Ensemble Transform Particle Filtering.” In: *SIAM Journal on Scientific Computing* 38.3 (2016), A1317–A1338. ISSN: 1064-8275. DOI: [10.1137/15M1038232](https://doi.org/10.1137/15M1038232).
- [25] P. Guttorp and T. Gneiting. “Studies in the history of probability and statistics XLIX: On the Matérn correlation family.” In: *Biometrika* 93 (2006), pp. 989–995. DOI: [10.1093/biomet/93.4.989](https://doi.org/10.1093/biomet/93.4.989).
- [26] W. Hackbusch. *Multi-Grid Methods and Applications*. Berlin Heidelberg: Springer-Verlag, 1985. ISBN: 978-3-540-12761-1. DOI: [10.1007/978-3-662-02427-0](https://doi.org/10.1007/978-3-662-02427-0).

- [27] E. Hallman, I. C. F. Ipsen, and A. K. Saibaba. “Monte Carlo Methods for Estimating the Diagonal of a Real Symmetric Matrix.” In: *SIAM Journal on Matrix Analysis and Applications* 44.1 (2023), pp. 240–269. ISSN: 0895-4798. DOI: [10.1137/22M1476277](https://doi.org/10.1137/22M1476277).
- [28] R. Hartley. “A More Symmetrical Fourier Analysis Applied to Transmission Problems.” In: *Proceedings of the IRE* 30.3 (1942), pp. 144–150. ISSN: 2162-6634. DOI: [10.1109/JRPROC.1942.234333](https://doi.org/10.1109/JRPROC.1942.234333).
- [29] S. Heinrich. “Monte Carlo Complexity of Global Solution of Integral Equations.” In: *Journal of Complexity* 14.2 (1998), pp. 151–175. ISSN: 0885-064X. DOI: [10.1006/jcom.1998.0471](https://doi.org/10.1006/jcom.1998.0471).
- [30] H. Hoel, K. J. H. Law, and R. Tempone. “Multilevel ensemble Kalman filtering.” In: *SIAM Journal on Numerical Analysis* 54.3 (2016), pp. 1813–1839. ISSN: 0036-1429. DOI: [10.1137/15M100955X](https://doi.org/10.1137/15M100955X).
- [31] A. Istratuca and A. Teckentrup. *Smoothed Circulant Embedding with Applications to Multilevel Monte Carlo Methods for PDEs with Random Coefficients*. 2023. DOI: [10.48550/arXiv.2306.13493](https://doi.org/10.48550/arXiv.2306.13493).
- [32] P. Kumar, C. W. Oosterlee, and R. P. Dwight. “A multigrid multilevel Monte Carlo method using high-order finite-volume scheme for lognormal diffusion problems.” In: *International Journal for Uncertainty Quantification* 7.1 (2017). ISSN: 2152-5080, 2152-5099. DOI: [10.1615/Int.J.UncertaintyQuantification.2016018677](https://doi.org/10.1615/Int.J.UncertaintyQuantification.2016018677).
- [33] P. Kumar, C. Rodrigo, F. J. Gaspar, and C. W. Oosterlee. “On Local Fourier Analysis of Multigrid Methods for PDEs with Jumping and Random Coefficients.” In: *SIAM Journal on Scientific Computing* 41.3 (2019), A1385–A1413. ISSN: 1064-8275. DOI: [10.1137/18M1173769](https://doi.org/10.1137/18M1173769).
- [34] O. P. Le Maître and O. M. Knio. *Spectral Methods for Uncertainty Quantification*. Scientific Computation. Dordrecht: Springer Netherlands, 2010. ISBN: 978-90-481-3519-6. DOI: [10.1007/978-90-481-3520-2](https://doi.org/10.1007/978-90-481-3520-2).
- [35] C. Lemieux. *Monte Carlo and Quasi-Monte Carlo Sampling*. Springer Series in Statistics. New York, NY: Springer, 2009. ISBN: 978-0-387-78164-8. DOI: [10.1007/978-0-387-78165-5](https://doi.org/10.1007/978-0-387-78165-5).
- [36] F. Lindgren, H. Rue, and J. Lindström. “An explicit link between Gaussian fields and Gaussian Markov random fields: the stochastic partial differential equation approach.” In: *Journal of the Royal Statistical Society: Series B (Statistical Methodology)* 73.4 (2011), pp. 423–498. ISSN: 1467-9868. DOI: [10.1111/j.1467-9868.2011.00777.x](https://doi.org/10.1111/j.1467-9868.2011.00777.x).
- [37] N. Lüthen, S. Marelli, and B. Sudret. “Sparse Polynomial Chaos Expansions: Literature Survey and Benchmark.” In: *SIAM/ASA Journal on Uncertainty Quantification* 9.2 (2021), pp. 593–649. DOI: [10.1137/20M1315774](https://doi.org/10.1137/20M1315774).
- [38] A. Maurais, T. Alsup, B. Peherstorfer, and Y. Marzouk. *Multi-Fidelity Covariance Estimation in the Log-Euclidean Geometry*. 2023. DOI: [10.48550/arXiv.2301.13749](https://doi.org/10.48550/arXiv.2301.13749). arXiv: [2301.13749](https://arxiv.org/abs/2301.13749) [cs, math, stat]. URL: <http://arxiv.org/abs/2301.13749> (visited on 02/03/2023).
- [39] A. Maurais, T. Alsup, B. Peherstorfer, and Y. Marzouk. *Multifidelity Covariance Estimation via Regression on the Manifold of Symmetric Positive Definite Matrices*. 2023. DOI: [10.48550/arXiv.2307.12438](https://doi.org/10.48550/arXiv.2307.12438). arXiv: [2307.12438](https://arxiv.org/abs/2307.12438) [cs, math, stat]. URL: <http://arxiv.org/abs/2307.12438> (visited on 07/27/2023).
- [40] M. D. McKay, R. J. Beckman, and W. J. Conover. “A Comparison of Three Methods for Selecting Values of Input Variables in the Analysis of Output from a Computer Code.” In: *Technometrics* 21.2 (1979), pp. 239–245. ISSN: 0040-1706. DOI: [10.2307/1268522](https://doi.org/10.2307/1268522).

- [41] P. Mycek and M. De Lozzo. “Multilevel Monte Carlo Covariance Estimation for the Computation of Sobol’ Indices.” In: *SIAM/ASA Journal on Uncertainty Quantification* 7.4 (2019), pp. 1323–1348. DOI: [10.1137/18M1216389](https://doi.org/10.1137/18M1216389).
- [42] H. N. Najm. “Uncertainty Quantification and Polynomial Chaos Techniques in Computational Fluid Dynamics.” In: *Annual Review of Fluid Mechanics* 41.1 (2009), pp. 35–52. DOI: [10.1146/annurev.fluid.010908.165248](https://doi.org/10.1146/annurev.fluid.010908.165248).
- [43] B. Peherstorfer, K. Willcox, and M. Gunzburger. “Survey of Multifidelity Methods in Uncertainty Propagation, Inference, and Optimization.” In: *SIAM Review* 60.3 (2018), pp. 550–591. ISSN: 0036-1445. DOI: [10.1137/16M1082469](https://doi.org/10.1137/16M1082469).
- [44] R. J. Purser, W.-S. Wu, D. F. Parrish, and N. M. Roberts. “Numerical Aspects of the Application of Recursive Filters to Variational Statistical Analysis. Part I: Spatially Homogeneous and Isotropic Gaussian Covariances.” In: *Monthly Weather Review* 131.8 (2003), pp. 1524–1535. ISSN: 1520-0493, 0027-0644. DOI: [10.1175//1520-0493\(2003\)131<1524:NAOTA0>2.0.CO;2](https://doi.org/10.1175//1520-0493(2003)131<1524:NAOTA0>2.0.CO;2).
- [45] A. Quarteroni and G. Rozza, eds. *Reduced Order Methods for Modeling and Computational Reduction*. Cham: Springer International Publishing, 2014. ISBN: 978-3-319-02089-1. DOI: [10.1007/978-3-319-02090-7](https://doi.org/10.1007/978-3-319-02090-7).
- [46] C. E. Rasmussen. “Gaussian Processes in Machine Learning.” In: *Advanced Lectures on Machine Learning: ML Summer Schools 2003, Canberra, Australia, February 2 - 14, 2003, Tübingen, Germany, August 4 - 16, 2003, Revised Lectures*. Ed. by O. Bousquet, U. von Luxburg, and G. Rätsch. Lecture Notes in Computer Science. Berlin, Heidelberg: Springer, 2004, pp. 63–71. ISBN: 978-3-540-28650-9. DOI: [10.1007/978-3-540-28650-9_4](https://doi.org/10.1007/978-3-540-28650-9_4).
- [47] C. E. Rasmussen and C. K. I. Williams. *Gaussian Processes for Machine Learning*. The MIT Press, 2005. ISBN: 978-0-262-25683-4. DOI: [10.7551/mitpress/3206.001.0001](https://doi.org/10.7551/mitpress/3206.001.0001).
- [48] C. P. Robert and G. Casella. *Monte Carlo Statistical Methods*. Springer Texts in Statistics. New York, NY: Springer, 2004. ISBN: 978-1-4419-1939-7. DOI: [10.1007/978-1-4757-4145-2](https://doi.org/10.1007/978-1-4757-4145-2).
- [49] D. Schaden and E. Ullmann. “Asymptotic Analysis of Multilevel Best Linear Unbiased Estimators.” In: *SIAM/ASA Journal on Uncertainty Quantification* 9.3 (2021), pp. 953–978. DOI: [10.1137/20M1321607](https://doi.org/10.1137/20M1321607).
- [50] D. Schaden and E. Ullmann. “On Multilevel Best Linear Unbiased Estimators.” In: *SIAM/ASA Journal on Uncertainty Quantification* 8.2 (2020), pp. 601–635. DOI: [10.1137/19M1263534](https://doi.org/10.1137/19M1263534).
- [51] W. H. A. Schilders, H. A. Van Der Vorst, J. Rommes, H.-G. Bock, F. De Hoog, A. Friedman, A. Gupta, H. Neunzert, W. R. Pulleyblank, T. Rusten, F. Santosa, A.-K. Tornberg, L. L. Bonilla, R. Mattheij, and O. Scherzer, eds. *Model Order Reduction: Theory, Research Aspects and Applications*. Vol. 13. Mathematics in Industry. Berlin, Heidelberg: Springer, 2008. ISBN: 978-3-540-78840-9. DOI: [10.1007/978-3-540-78841-6](https://doi.org/10.1007/978-3-540-78841-6).
- [52] R. Shapiro. “Smoothing, filtering, and boundary effects.” In: *Reviews of Geophysics* 8.2 (1970), pp. 359–387. ISSN: 1944-9208. DOI: [10.1029/RG008i002p00359](https://doi.org/10.1029/RG008i002p00359).
- [53] L. M. Stein. *Interpolation of Spatial Data*. Springer-Verlag, New York, NY, 1999.
- [54] R. K. Tripathy and I. Bilonis. “Deep UQ: Learning Deep Neural Network Surrogate Models for High Dimensional Uncertainty Quantification.” In: *Journal of Computational Physics* 375 (2018), pp. 565–588. ISSN: 0021-9991. DOI: [10.1016/j.jcp.2018.08.036](https://doi.org/10.1016/j.jcp.2018.08.036).
- [55] U. Trottenberg, C. W. Oosterlee, and A. Schuller. *Multigrid*. Elsevier, 2000. ISBN: 978-0-08-047956-9. URL: <https://www.elsevier.com/books/multigrid/trottenberg/978-0-08-047956-9>.

- [56] A. T. Weaver and I. Mirouze. “On the diffusion equation and its application to isotropic and anisotropic correlation modelling in variational assimilation.” In: *Quarterly Journal of the Royal Meteorological Society* 139.670 (2013), pp. 242–260. ISSN: 1477-870X. DOI: [10.1002/qj.1955](https://doi.org/10.1002/qj.1955).
- [57] A. T. Weaver, J. Tshimanga, and A. Piacentini. “Correlation Operators Based on an Implicitly Formulated Diffusion Equation Solved with the Chebyshev Iteration.” In: *Quarterly Journal of the Royal Meteorological Society* 142.694 (2016), pp. 455–471. ISSN: 1477-870X. DOI: [10.1002/qj.2664](https://doi.org/10.1002/qj.2664).
- [58] A. Weaver and P. Courtier. “Correlation modelling on the sphere using a generalized diffusion equation.” In: *Quarterly Journal of the Royal Meteorological Society* 127.575 (2001), pp. 1815–1846. ISSN: 1477-870X. DOI: [10.1002/qj.49712757518](https://doi.org/10.1002/qj.49712757518).
- [59] A. T. Weaver, M. Chrust, B. Ménérier, and A. Piacentini. “An evaluation of methods for normalizing diffusion-based covariance operators in variational data assimilation.” In: *Quarterly Journal of the Royal Meteorological Society* 147.734 (2021), pp. 289–320. ISSN: 1477-870X. DOI: [10.1002/qj.3918](https://doi.org/10.1002/qj.3918).
- [60] P. Whittle. “Stochastic processes in several dimensions.” In: *Bull. Inst. Internat. Statist.* 40 (1963), pp. 974–994.
- [61] R. Wienands. *Practical Fourier Analysis for Multigrid Methods*. Chapman and Hall/CRC, 2004. ISBN: 978-0-429-14328-1. DOI: [10.1201/9781420034998](https://doi.org/10.1201/9781420034998).
- [62] D. Xiu. *Numerical Methods for Stochastic Computations: A Spectral Method Approach*. Princeton University Press, 2010. ISBN: 978-0-691-14212-8. DOI: [10.2307/j.ctv7h0skv](https://doi.org/10.2307/j.ctv7h0skv).